Description of Communication System Options for Single-Aperture Multiple-Link (SAML) Mission Support

H. Tsou, S. Million, S. M. Hinedi, T. M. Nguyen, M. K. Simon, and W. V. Moore
Communications Systems and Research Section

S. Kayalar
Spacecraft Telecommunications Equipment Section

R. L. Horttor
Telecommunications Science and Engineering Division

This article presents five communication system options for single-aperture multiple-link (SAML) mission support that are capable of supporting a multiplicity of spacecraft that are simultaneously within the beamwidth of a single ground-station antenna. These proposed system options provide both short-term and long-term solutions for future deep-space missions such as MarsNet and the Mars Surveyor Program. The article describes these options in detail and also identifies issues and potential limitations associated with each option. Preliminary solutions are provided to some of these issues, and a set of recommendations regarding which system options are suitable for SAML scenarios is also presented.

I. Introduction

A. Background

Presently, there are several proposed future missions to Mars, e.g., the Mars Surveyor Program (MSP) and MarsNet, that involve multiple spacecraft. The MSP network comprises about 10 to 12 small landing vehicles distributed over the Martian surface to form a global network, with proposed launch dates of 1998, 2001, and 2003. On the other hand, MarsNet, consisting of 3 or 4 small landers with a proposed launch date of January 2001, is a joint National Aeronautics and Space Administration (NASA) and European Space Agency (ESA) mission that will complement the MSP network in its investigation of Mars. For these missions, it is highly possible that more than one spacecraft (S/C) will be within the same beamwidth of a single Deep Space Network (DSN) ground antenna (see Fig. 1). This condition provides the opportunity to communicate with multiple S/C using a single antenna, with considerable operational cost savings over the use of multiple antennas. A preliminary investigation [1] has identified two system options capable of tracking several S/C from a single Earth station using a single Earth-to-space link (uplink) and multiple space-to-Earth links (downlinks). These two proposed system options employ Consultative Committee for Space Data Systems (CCSDS) packetized telecommand [2] for the uplink and either adjustable turnaround frequency ratios or subcarrier frequency division multiple access

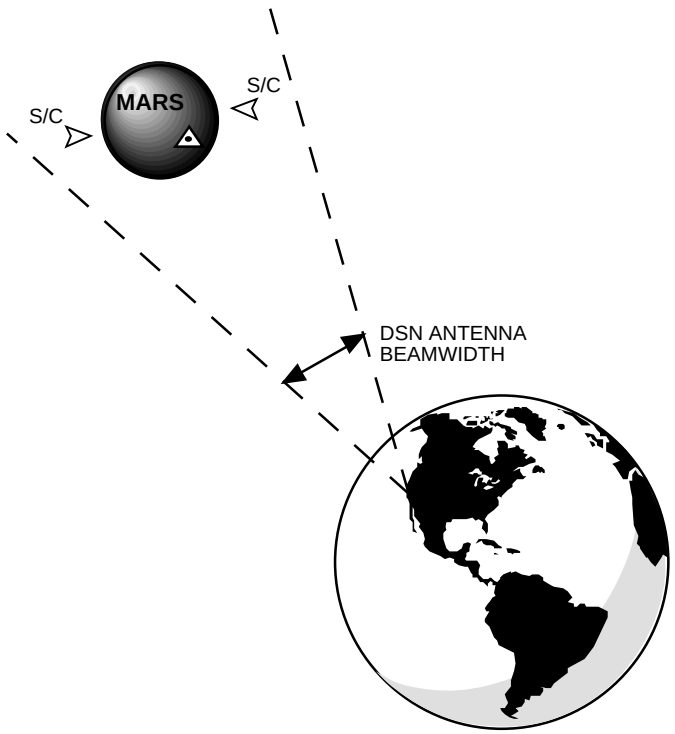

Fig. 1. A typical scenario for multiple S/C support with a single DSN ground antenna.

with fully suppressed carrier for the downlink. Recently, three more system options have been identified for SAML mission support. All of these five system options to be discussed in this article involve various degrees of modification to the current S/C transponder and DSN ground-station system design. A list of these five system options prioritized in terms of the required modification to the current system for each option, e.g., option no. 1 requires the least modifications while option no. 5 requires the most modifications, is provided here as an overview.

(1) Option no. 1:
Uplink: CCSDS packetized telecommand (CCSDSPT).
Downlink: Subcarrier frequency division multiple access (SFDMA).

(2) Option no. 2:
Uplink: CCSDSPT and subcarrier frequency division multiplexing (SFDM).
Downlink: SFDMA.

(3) Option no. 3:
Uplink: CCSDSPT.
Downlink: Carrier frequency division multiple access (CFDMA) with adjustable turnaround frequency ratios (ATFR).

(4) Option no. 4:
Uplink: CCSDSPT.
Downlink: Code division multiple access (CDMA) with pseudorandom noise (PN) codes.

(5) Option no. 5:
Uplink: Code division multiplexing (CDM) with Walsh–Hadamard function.
Downlink: CDMA with PN codes.

Besides the above-mentioned system options, transmitting multiple uplink carriers by a single DSN antenna is another candidate for the SAML uplink support. This uplink option can work with any of the uplink options mentioned above. However, self-interference in the forms of broadband noise burst and coherent intermodulation products can happen when multiple carriers are added and transmitted together at S-band (2.2–2.3 GHz) [3], and the effects causing self-interference are highly dependent on the physical configuration and condition of the antenna in use. Based on the recent experiment results gathered from a 34-m DSN antenna (DSS 13) at X-band (8.4–8.5 GHz) [4], it is estimated that a 6-dB power back-off is required to support two uplink carriers without causing noticeable noise bursts and intermodulation products. Here, we will not include this multiple-uplink option, mainly because of the fact that it can be used in conjunction with any of those uplink options discussed later in this article. Although it can also be used alone, the readers are cautioned here that there is a power back-off required to alleviate the self-interference problem.

B. Typical Link Performance For Mars Missions—An Example

To determine the suitability of the previously mentioned system options for supporting the SAML scenarios, one needs to know the telecommunication link performance of the missions. For the proposed Mars missions, the telecommunication link design control tables (DCTs) were run for typical X-band uplink and downlink scenarios, and some sample links are included in Appendix A. The Mars orbiters in this analysis were assumed to use a 1.5-m high-gain antenna (HGA) with a gain of 38.6 dBi to support 500-bps and 2-kbps uplink telecommand data rates as well as 10-kbps and 20-kbps downlink telemetry data rates, with a range up to 2.67 astronomical units (AU). The Mars landers were assumed to use a low-gain antenna (LGA) with a gain of 9.2 dBi to support downlink data rates at 10 bps and 40 bps. Also, the Viterbi (7,1/2) encoded downlink telemetry and standard modulation schemes, i.e., pulse code modulation/phase shift keying/phase modulation (PCM/PSK/PM) with sine-wave subcarrier for the uplink and square-wave for the downlink [5], were assumed for the analysis.

The performance margins for the telecommand data, assuming a 20-kW DSN 34-m high-efficiency (HEF) antenna, obtained from the DCTs given in Appendix A, were 25.82 dB for the orbiter and −2.18 dB for the lander at a data rate of 500 bps (and additionally 6-dB lower for a data rate of 2 kbps) when the bit-error rate (BER) is fixed at 10^{-5}. This indicates that a DSN 34-m HEF antenna will not have enough margin to command the lander at these specified data rates all the way out to the maximum range. Therefore, unless the data rate can be relaxed, a DSN 70-m antenna, which has about 6-dB higher antenna gain than the 34-m antenna, is required to support data rates up to 500 bps for the lander, if required by the missions. On the other hand, the downlink margins for the orbiters were 3.17 dB for 20 kbps (or 3-dB higher for 10 kbps) and −0.37 dB for 40 bps (or 3-dB higher for 20 kbps) for the landers. Therefore, the landers will not be able to communicate with a DSN 34-m HEF station at 40 bps for the given link conditions, and a DSN 70-m antenna is required to support the landers for data rates higher than 20 bps.

Another set of parameters that is also important in determining the suitable communication system to support the SAML scenarios is the Doppler profile (Doppler and Doppler rate). The Doppler calculations for a Mars orbiter in an elliptical orbit were made for the worst case. The calculations are conservative but provide an upper bound for transponder designers to use in determining DSN telemetry channelization for the S/C transponder. The worst-case one-way Doppler was found to be 97.4 kHz, and the worst-case Doppler rate was found to be ±50 Hz/s. The Doppler profiles are included in Appendix B.

Based on this estimate, this article extends the work presented in [1] to include (1) a more detailed description of the two options proposed in the previous work and (2) a study of three more system options that can support SAML scenarios. The detailed system descriptions of these options will be presented in the following five sections, with issues and potential problems associated with each option being identified at the end of each section. The performance of the uplink and downlink options are then separately compared. The recommendations and conclusions are presented in the last section.

II. Description of System Option No. 1

The proposed system option no. 1 employs the CCSDS packet telecommand (CCSDSPT) on the uplink and subcarrier frequency division multiple access (SFDMA) on the downlink. Figures 2(a) and 2(b) depict simplified block diagrams for this proposed system architecture.

On the uplink, telecommands for all S/C are formatted using a CCSDS packet telecommand, and the command packet stream is then binary phase-shift keyed on the sine-wave subcarrier, which in turn phase modulates the RF residual carrier [see Fig. 2(a)]. This is the CCSDS standard for uplink telecommand, and it is referred to as the PCM/PSK/PM modulation format with a sine-wave subcarrier [5], which can be described mathematically as

$$S_u(t) = \sqrt{2P_u}\sin(2\pi f_u t + m_u d_u(t)\sin(2\pi f_{sc} t)) \tag{1}$$

where P_u is the uplink power; m_u denotes the uplink command modulation index; f_u is the uplink frequency; $d_u(t)$ is the binary, nonreturn-to-zero (NRZ)-formatted composite telecommand data waveform; and f_{sc} denotes the telecommand subcarrier frequency. The spectrum of this signal is shown in Fig. 2(c).

The uplink telecommand signal is sent using a single residual-carrier RF frequency (f_u) from a single DSN antenna, and it will be received by all S/C that lie within the Earth station antenna's beamwidth. All S/C carrier tracking loops try to acquire and track the uplink carrier [see Fig. 2(a)]. After the carrier demodulation, the signal is processed by a standard NASA deep-space command detector unit (CDU),[1] which is a coherent demodulator for an NRZ data stream that is binary phase-shift keyed (BPSK) onto a sinusoidal subcarrier at a frequency of either 8 kHz or 16 kHz. After the command demodulation, the CCSDS packet telecommand will be processed to separate the command data on the uplink. Since the CCSDS telecommand format allows addressing of both S/C and instruments [2], only commands addressed to a specific S/C will be responded to by that S/C after identification (ID) verification. Command data are then routed to various subsystems whose addresses appear in the segment or packet headers [6].

Figure 3(a) shows a standard telecommand data structure consisting of multiple command link transmission units (CLTUs); each starts with a 16-bit start sequence followed by the encoded telecommand data organized into fixed-length telecommand code blocks and ends with a tail sequence that is constructed specifically to be a noncorrectable code block delimiting the end of a CLTU by stopping the decoding process and forcing the CDU into the search mode of a start sequence. The start sequence, for single S/C support, is a fixed synchronization pattern used to delimit the beginning of a CLTU and resolve the data ambiguity (sense of "1" and "0"). It is designed to have very good autocorrelation characteristics (i.e., small autocorrelation side lobes) for delimiting purposes; therefore, only a few valid start sequence candidates are available.[2] On the receiving end, the telecommand decoding process will not commence until the start sequence pattern is positively identified in the received bit stream. Therefore, for SAML support, the start sequence can also be used to distinguish the intended receiving S/C from the others by assigning a unique start sequence to each supported S/C. This additionally requires very good cross-correlation properties among the start sequences used in SAML support for the protection of false identification, which can pose a great challenge to the selection of start sequences when the number of supported S/C increases. A code block, identified as the smallest unit in the coding layer data structure, is a fixed-length bit stream containing the coded telecommands. As shown in Fig. 3(b), a code block consists of 56 information bits (32, 40, or 48 bits for a shortened code block) and 7 error control bits, formulated by using a modified single-error-correcting, double-error-detecting Bose–Chaudhuri–Hocquenghem (BCH) block

[1] J. B. Berner, *NASA Deep Space Command Detector Unit Development—Final Engineering Report*, JPL D-4233 (internal document), Jet Propulsion Laboratory, Pasadena, California, June 9, 1987.

[2] The bit pattern of "1110 1011 1001 0000" is currently recommended by CCSDS as a start sequence in telecommand CLTU.

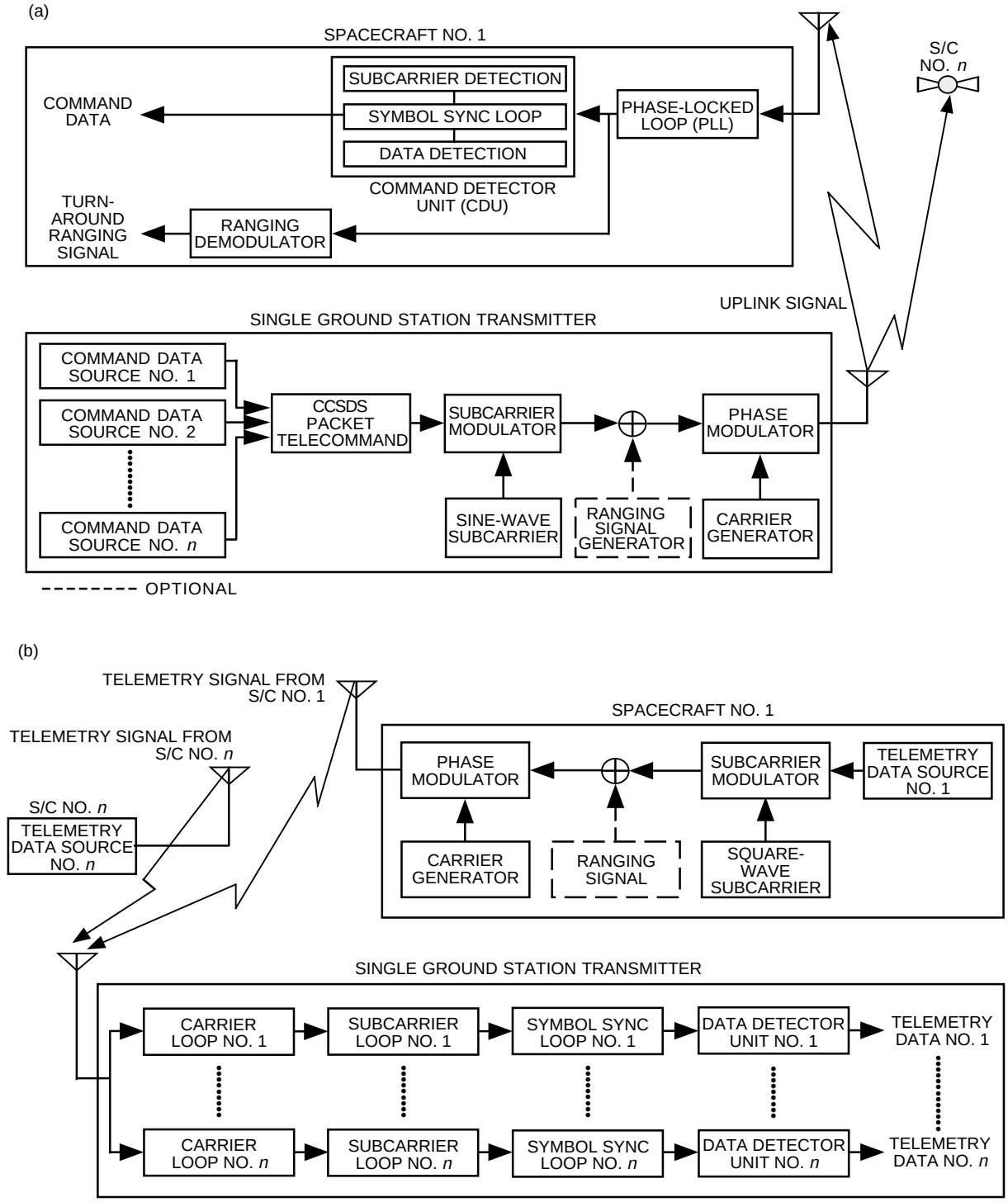

Fig. 2. System option no. 1: (a) a simplified block diagram of the CCSDSPT uplink, (b) a simplified block diagram of the SFDM downlink, (c) the spectrum of the uplink signal without the ranging signal, and (d) the spectrum of the downlink signal without the ranging signal.

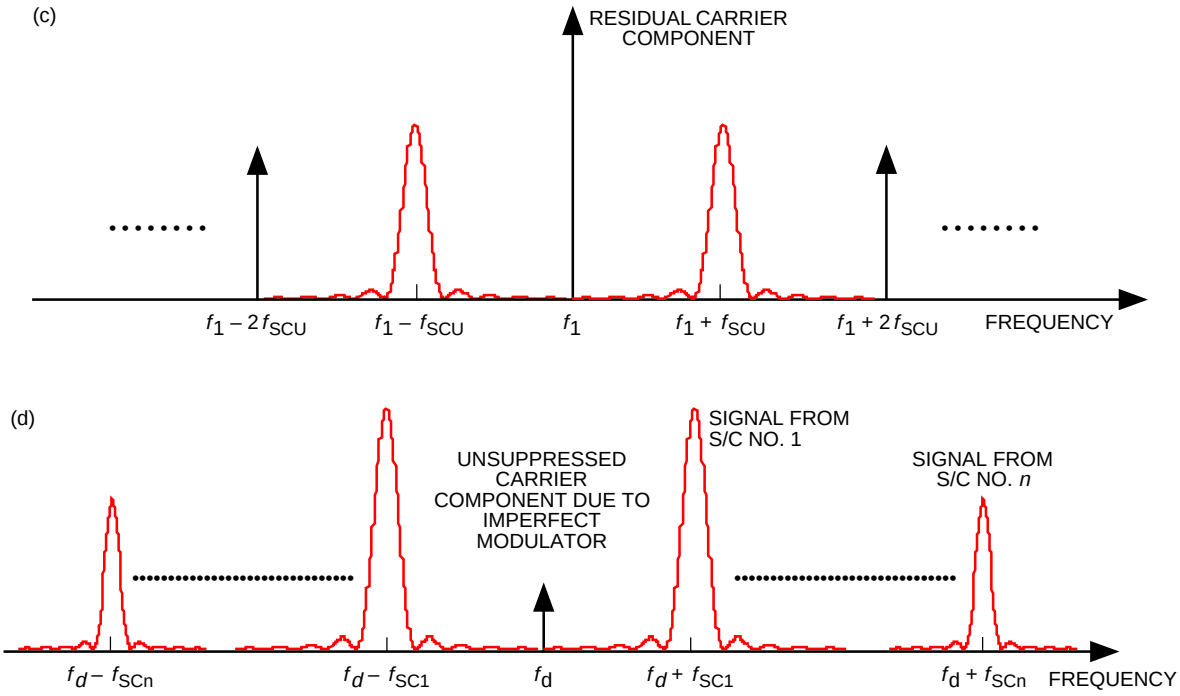

Fig. 2 (cont'd). System option no. 1: (a) a simplified block diagram of the CCSDSPT uplink, (b) a simplified block diagram of the SFDM downlink, (c) the spectrum of the uplink signal without the ranging signal, and (d) the spectrum of the downlink signal without the ranging signal.

code, as well as a trailing fill bit. A frame, on the contrary, is a logical unit on the data transfer layer that is assembled from one or more code blocks. There can be more than one frame assembled from a CLTU; however, one frame per CLTU is a natural choice when a unique start sequence for each supported S/C is implemented as suggested. Figure 3(c) depicts the transfer frame format, which includes a 10-bit spacecraft ID field in its frame header for S/C identification purposes and 2 spare bits that can be designated for SAML support. Using a unique ID in the frame header for each S/C can provide additional isolation on the data transfer layer among supported S/C to ensure the correct delivery of telecommand packets.

To separate the downlink channels, this system uses a single downlink RF carrier frequency with the downlink telemetry signals each placed on a different subcarrier frequency. This is referred to as subcarrier frequency division multiple access (SFDMA). Figure 2(b) shows a simplified block diagram for the SFDMA downlink system. The telemetry data from the ith S/C is phase-shift keyed on the ith square-wave subcarrier, which is then phase modulated on a suppressed RF carrier. This is fully compatible with the CCSDS standard downlink signal format [5], i.e., the so-called PCM/PSK/PM modulation with a square-wave subcarrier, and is expressed mathematically as

$$S_{d_i}(t) = \sqrt{2P_{d_i}}\sin(2\pi f_d t + m_{d_i} d_i(t) Sq(2\pi f_{sc_i} t)) \tag{2}$$

where f_d is the downlink carrier frequency; m_{d_i} denotes the downlink telemetry modulation index for the ith S/C, which is set at $\pi/2$ when the carrier is fully suppressed; P_{d_i} is the downlink power for the ith S/C; $d_i(t)$ is the telemetry data from the ith S/C; and f_{sc_i} is the telemetry subcarrier frequency of the ith S/C. The spectrum plot for the downlink signal is shown in Fig. 2(d).

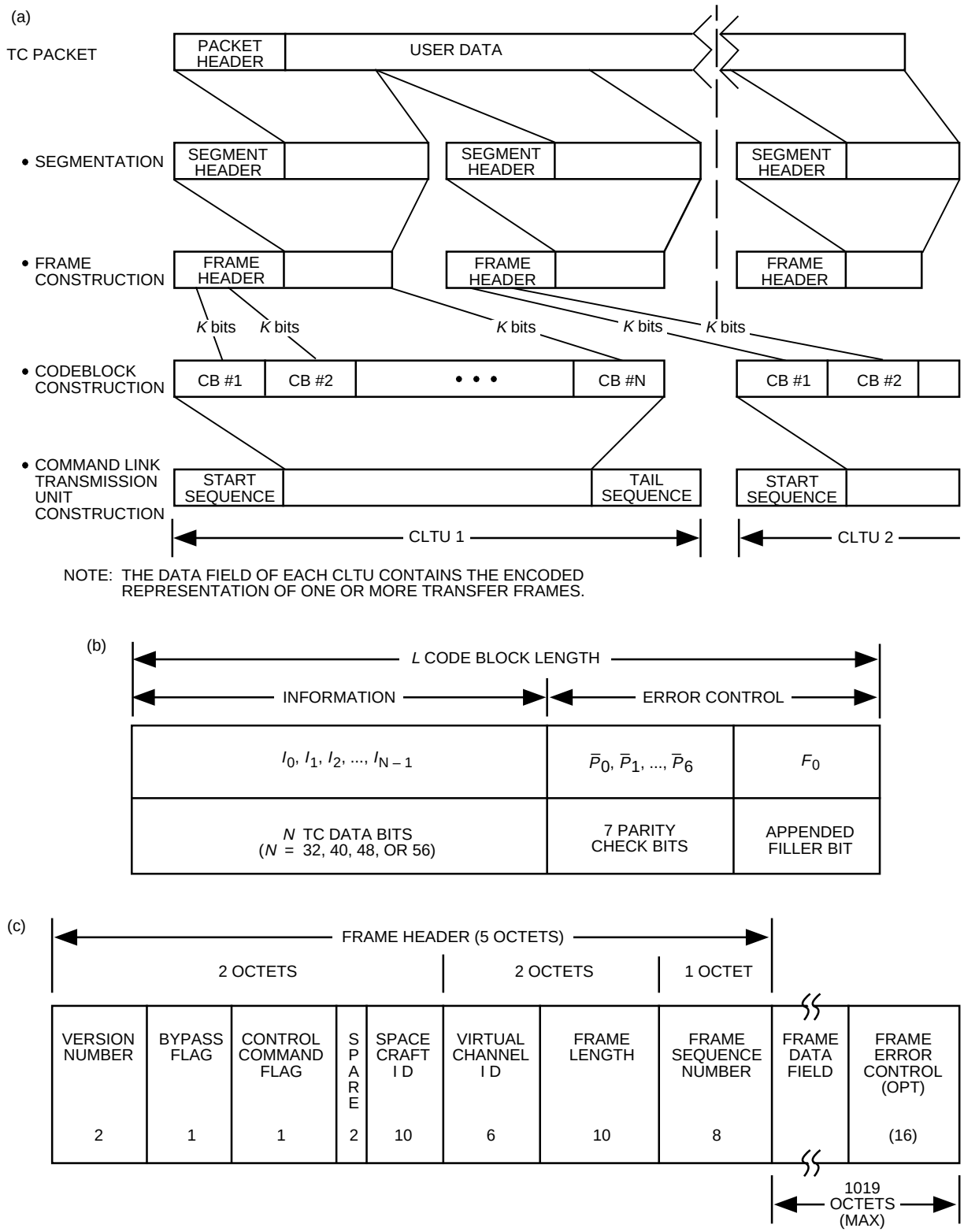

Fig. 3. Telecommand (a) data structure, (b) code block format, and (c) transfer frame format (1 octet is an 8-bit data string).

As shown in Fig. 2(b), a single ground station can demodulate the received signal by routing it into a bank of DSN receivers that are tuned to the common carrier frequency with their respective subcarrier frequencies corresponding to each supported spacecraft. Each receiver has its own carrier, subcarrier, and symbol synchronization loops to provide coherent carrier/subcarrier demodulation capability. Finally, the telemetry data can be extracted by a data detector, which consists of an integrate-and-dump circuit and a threshold detector.

There are various issues and potential limitations associated with this option, e.g., uplink carrier acquisition, CCSDS frame header design, unsuppressed-carrier components and interchannel interference among active downlinks, and simultaneous command/ranging/telemetry operations. These issues will be discussed in the following sections.

A. Uplink Carrier Acquisition

With a single S/C link, the uplink carrier acquisition traditionally is done by sweeping the uplink frequency of an unmodulated carrier from the ground station. The phase-locked loop (PLL) on board the S/C acquires and locks on the carrier when frequency is swept through its best lock frequency. This procedure is part of a telecommand session consisting of different carrier modulation modes (CMMs) [2] representing different states of data modulation on the RF carrier that creates the physical telecommand channel. Figure 4 depicts the sequence of CMMs comprising the physical layer operations procedure-2 (PLOP-2), in which the carrier acquisition by frequency sweeping occurs in step 1 and the telecommand channel is not required to be deactivated after each transmitted CLTU. The optional idle sequence is a high transition-density bit pattern which, when used, can help to maintain channel symbol synchronization between transmitted CLTUs.

One major issue in the frequency-sweeping acquisition is that the S/C receiver pull-in time, lock-in time, mean time between drop locks, probability of staying in lock, and maximum sweep rate that can be tracked by a receiver PLL, etc., are all functions of the received uplink power, since the receiver PLL bandwidth is dynamically determined by the received power. Several potential problems become inevitable when the frequency-sweeping acquisition technique is employed in the SAML scenarios. For example, the sweep rate must be kept low to accommodate S/C with the weakest received power, such as landers using low-gain antennas. Also, the frequency range needed to be swept would be larger since it has to include the best lock frequencies of all the S/C, which may be experiencing totally different dynamics. Therefore, the uplink carrier acquisition for SAML support is expected to take more time.

Figure 5 shows the normalized PLL pull-in time, the probability of staying in lock, and the maximum sweep rate that can be tracked versus the uplink received power. The results indicate that for Mars mission parameters and typical operating conditions of the deep-space transponder (DST), the receiver PLL will acquire and stay in lock on the uplink frequency with certainty for the Mars orbiters at the estimated uplink received power of -112 dBm (see Appendix A). For the Mars landers, even though the acquisition will be slow at the estimated received power of -140 dBm, the receiver PLL almost certainly will stay in lock. The maximum sweep rate for SAML support of such a Mars mission will not be higher than 1700 Hz/s, even though the orbiter can sustain a higher sweep rate of up to 5000 Hz/s.[3]

Another potential problem with this frequency-sweeping acquisition technique is that it does not provide flexibility for the additional S/C to acquire the uplink if they come in view after the start of the telecommand session, or to reacquire a previously established uplink if the signal is lost during transmission. This is due to the uplink frequency being swept by the ground station for the traditional single S/C support. With multiple S/C, it is better to maintain a constant uplink frequency while allowing S/C to sweep their internal references. This transfer of frequency sweeping from ground station to S/C allows truly independent uplinks in that, if reacquisition by a S/C is needed,

[3] The maximum sweep rates quoted here represent the full capacity of the transponders. By maintaining a margin, the DSN is usually operating at a sweep rate that is much less than the maximum capacity.

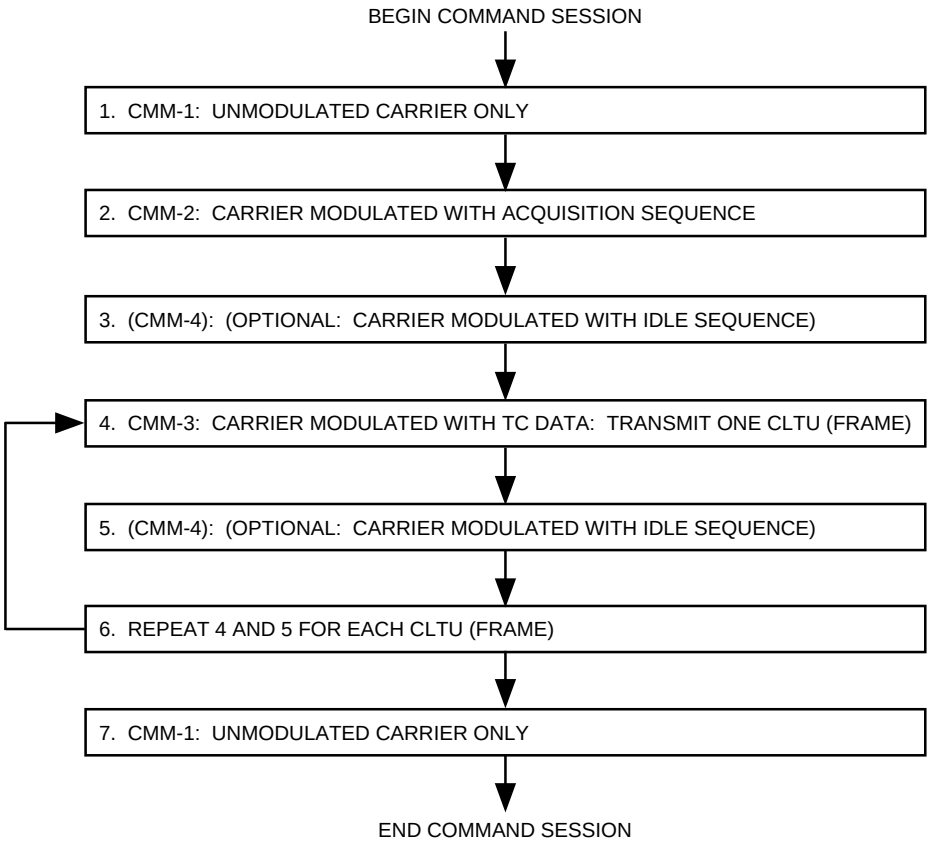

Fig. 4. The recommended carrier modulation mode (CMM) sequence on the physical layer.

there is no need to interrupt other established links. However, this requires better processing on board S/C, and these smarter transponder features should be incorporated in the Small DST and the Tiny DST currently under development.

B. CCSDS Packet Header

One of the major concerns for the CCSDSPT uplink option is the number of S/C that can be supported by the current CCSDS standard. In principle, one can find out the answer only after calculating the probabilities of false frame rejection and false frame delivery for each S/C. A false frame rejection happens when either a matching start sequence is wrongly rejected or, after telecommand decoding, any of the code blocks in a frame is rejected because of not being able to be decoded. As described earlier, each code block is individually encoded on the coding layer with a single-error-correcting double-error-detecting BCH code. The probability of one or more code blocks of a CLTU being rejected becomes

$$P_E(CB) = 1 - \left[(1-P_b)^{L-1} + (L-1)P_b(1-P_b)^{L-2}\right]^M \tag{3}$$

where P_b is the channel bit-error probability, L is the length of the code block in bits (including the trailing fill bit), and M is the number of code blocks in a CLTU. On the transfer layer, a code block rejection anywhere in a frame will result in the rejection of the whole frame. For the single-frame-per-CLTU case in the SAML scenario, the probability of a false frame rejection becomes

$$P_E(FR) = P_E(SS) + [1 - P_E(SS)]P_E(CB) \tag{4}$$

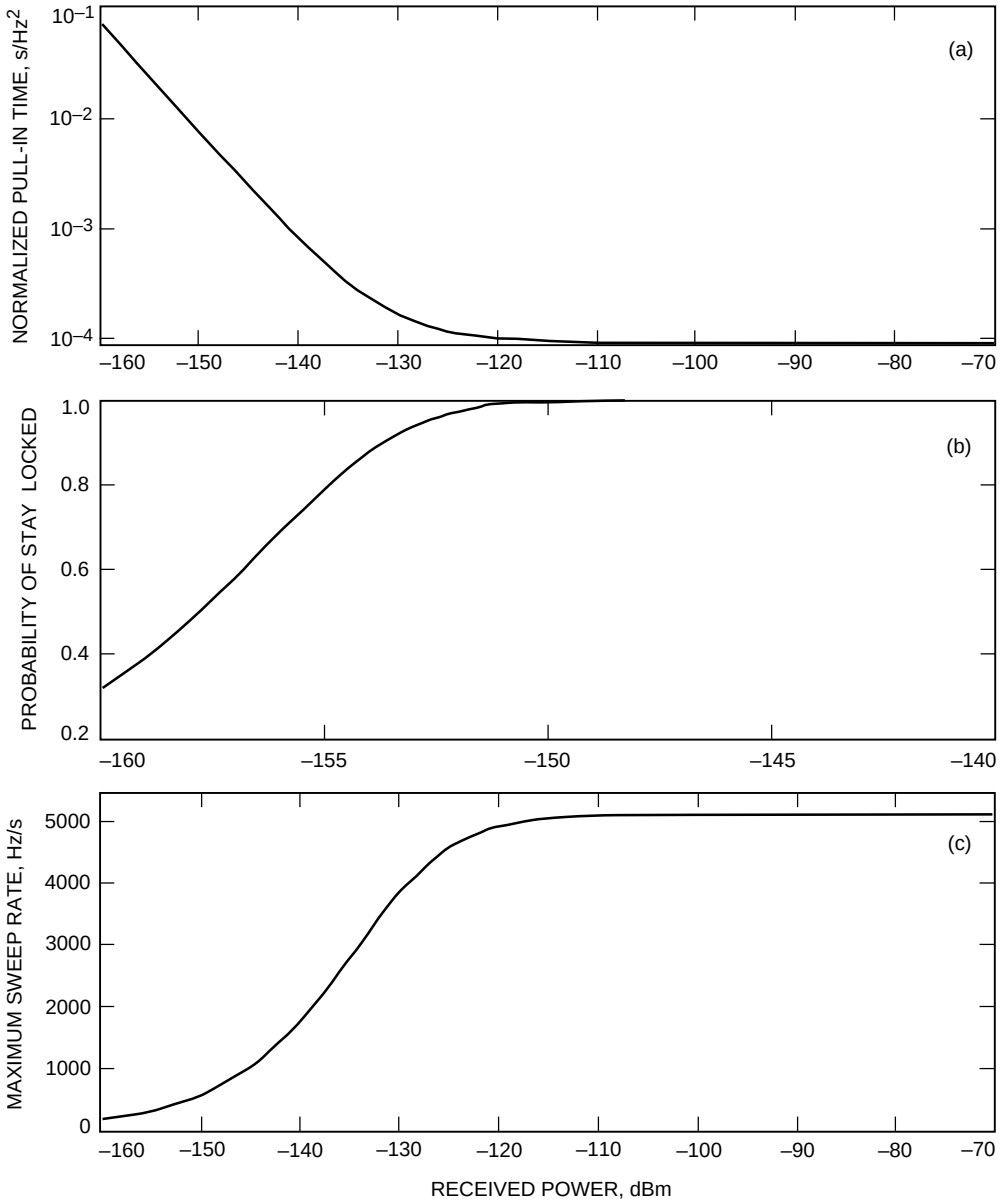

Fig. 5. Uplink carrier acquisition performance: (a) normalized pull-in time, (b) probability of staying in lock, and (c) maximum sweep rate.

where $P_E(SS)$ is the probability of rejecting the start sequence of a CLTU that is addressed specifically to the intended receiving S/C. For zero-error tolerance in a 16-bit start sequence detection, we have

$$P_E(SS) = 1 - (1 - P_b)^{16} \tag{5}$$

On the other hand, a false frame delivery can only happen when both the CLTU start sequence and the S/C ID in the transfer frame header are misidentified as those assigned for another S/C. Since the frame has to be good for delivery, each code block, including the one containing the frame header, must be decoded successfully. The probability of false frame delivery can be bounded as

$$P_{FD}(FR) \le P_{FD}(SS)P_{FD}(ID)\left[(1-P_b)^{L-1} + (L-1)P_b(1-P_b)^{L-2}\right]^{M-1} \tag{6}$$

where $P_{FD}(ID)$ and $P_{FD}(SS)$ are the false detection probabilities of the S/C ID in the transfer frame and the CLTU start sequence, and they are dependent, respectively, on the minimum distance between the assigned start sequences and S/C IDs among all the users in an SAML mission. According to the Plotkin bound [7], the largest minimum distance achievable, d_{min}, among all possible subsets, each containing N distinct n-bit sequences, is bounded as

$$d_{min} \le \begin{cases} \left\lfloor \frac{n}{2}\left(\frac{N}{N-1}\right)\right\rfloor & \text{for even } N \\ \left\lfloor \frac{n}{2}\left(\frac{N+1}{N}\right)\right\rfloor & \text{for odd } N \end{cases}$$

Hence, with a properly selected set of S/C IDs, the false detection probability of the 10-bit S/C ID should be bounded as

$$P_{FD}(ID) = 1 - \sum_{k=0}^{\lfloor \frac{d_{min}-1}{2} \rfloor} \binom{10}{k} P_b^k (1-P_b)^{10-k}$$

Based upon the Levenshtein construction method using Hadamard matrices and a code-puncturing technique [7], a set of six 10-bit S/C IDs with $d_{min} = 6$ and a set of twelve 10-bit S/C IDs with $d_{min} = 5$ can be realized. Both sets meet the Plotkin bound with double-error-correcting capability, and the former also has triple-error-detecting capability. With typical $P_b \le 10^{-5}$ scenarios, the false identification on the S/C ID is very unlikely for these code sets, even if the misidentification of a start sequence is highly probable. A common CLTU start sequence may be shared by this relatively small number of S/C in this case. For even a higher number of users in an SAML support, the 10-bit shortened Hamming codes [8] with $d_{min} = 4$ can support up to 64 users, with the capability of single-error correction and double-error detection. It is suggested a unique 16-bit CLTU start sequence for each S/C be used in this case as an additional measure to keep the false detection probability low.

With the number of S/C proposed for Mars missions, one can say with confidence that the current CCSDS standard using a common 16-bit CLTU start sequence and a unique 10-bit ID for each S/C in the frame header is sufficient to support Mars missions with a maximum number of S/C around 16, and the chance of having all the S/C lie within the same beamwidth is slim, assuming that they are uniformly distributed in the orbit. With the suggested use of the combination of a unique 16-bit CLTU start sequence and a 10-bit S/C ID for each S/C, the additional degree of protection on the coding layer can improve the insulation among all the users, which allows even more users into SAML scenarios. It is noted that a subset of Kasami or Bent sequences [12] can serve for the required CLTU start sequences because of their excellent autocorrelation and cross-correlation properties. Also, for SAML support, it is recommended that one spare bit in the frame header be used to indicate that the SAML is in operation and the frame error control used for error control is in the frame.

C. Unsuppressed-Carrier Components in the Downlink

Unsuppressed (discrete) carrier components generated by nonideal phase modulators [see Fig. 2(d)] employed by the S/C transponder potentially can cause, depending on their implementation, performance degradation at the ground station over and above that due to the power lost in the discrete component itself. If, for example, the modulation is generated from the difference of two 100-percent binary amplitude modulations (AMs) where the AMs themselves are the inverse of each other, then if

the two AM modulators are not perfect, i.e., they exhibit amplitude and phase imbalances, then the resultant difference signal will contain an undesired discrete carrier component in phase with the desired suppressed-carrier component. If, on the other hand, the modulation is formed by directly phase modulating a carrier with the binary data modulation, then if the modulation angle is other than ideal, i.e., less than 90 deg, then again an undesired discrete spectral component will be generated that is now in phase quadrature with the desired suppressed-carrier data modulation component. Either of these two implementations would produce a degradation, i.e., increase in tracking jitter, in the Costas loop that is used to track the suppressed-carrier component of the downlink RF signal. In the case where multiple signals are transmitted, however, each data signal is first modulated onto a subcarrier before being modulated onto the RF carrier. Here the second of the above two implementations is the likely candidate, namely, each data-modulated subcarrier is phase modulated onto the RF carrier. In this case, there will be an unsuppressed-carrier component that is in phase quadrature with the desired suppressed-carrier components. However, because of the baseband modulation onto subcarriers, it is easily shown (see Appendix C) that the discrete components generated will not degrade the performance of the Costas loop if the subcarrier frequencies are large with respect to the data rate and integrate-and-dump (I&D) arm filters are used in the loop.

D. Interchannel Interference in the Downlink

Since various subcarriers are used to separate the downlink telemetry signal, the potential for interference among the data channels exists. To minimize the interchannel interference, the guard band between the channels has to be chosen carefully so that all information concerning local frequency drift, two-way Doppler, and Doppler rate are taken into consideration. This means that the downlink subcarrier frequencies should be selected properly to avoid interchannel interference in the presence of frequency drift and two-way Doppler/Doppler rate.

E. Simultaneous Command/Ranging/Telemetry Operations

In order to reduce operation time, simultaneous command/ranging/telemetry is recommended for SAML. According to Recommendation 401 (3.4.1) B-1 [5], the DSN requests that all future S/C designed permit simultaneous telecommand/ranging/telemetry operations whenever these services are required by the missions. This means that, if it is required, all telecommanding and ranging should be completed within the time scheduled for telemetry data dumps so that no additional DSN passes will be required for these purposes. However, simultaneous operation creates the potential for interferences among the command, ranging, and telemetry channels. In order to minimize the interferences among these channels, proper frequency planning for the subcarrier and selection of telemetry modulation indices are required [9].

F. Performance of System Option No. 1

If the system was designed properly, i.e., proper choice of modulation indices, subcarrier frequencies, subcarrier waveforms, carrier and subcarrier tracking algorithms, etc., the performance of option no. 1 would be very similar to the performance of the current systems recommended by the CCSDS. The uplink system performance is identical to the current standard single S/C uplink systems but, from each spacecraft's point of view, at a smaller data throughput, since all the S/C are indeed time sharing the uplink with packetized telecommand. The symbol error rate (SER) performance for a standard uplink system utilizing the CCSDS packet is shown in Fig. 6(a), where typical operating conditions with P_u/N_0 ranging between 44 and 54 dB-Hz, a command data rate of 2 kbps, a command modulation index of 70 deg, a sine-wave subcarrier frequency of 32 kHz, and the same loop SNRs of at least 22 dB for both the analog carrier-tracking PLL and the data-aided subcarrier tracking loop are assumed. Under these operating conditions, the bit SNR degradation shown in Fig. 6(a) is about 0.2 dB.

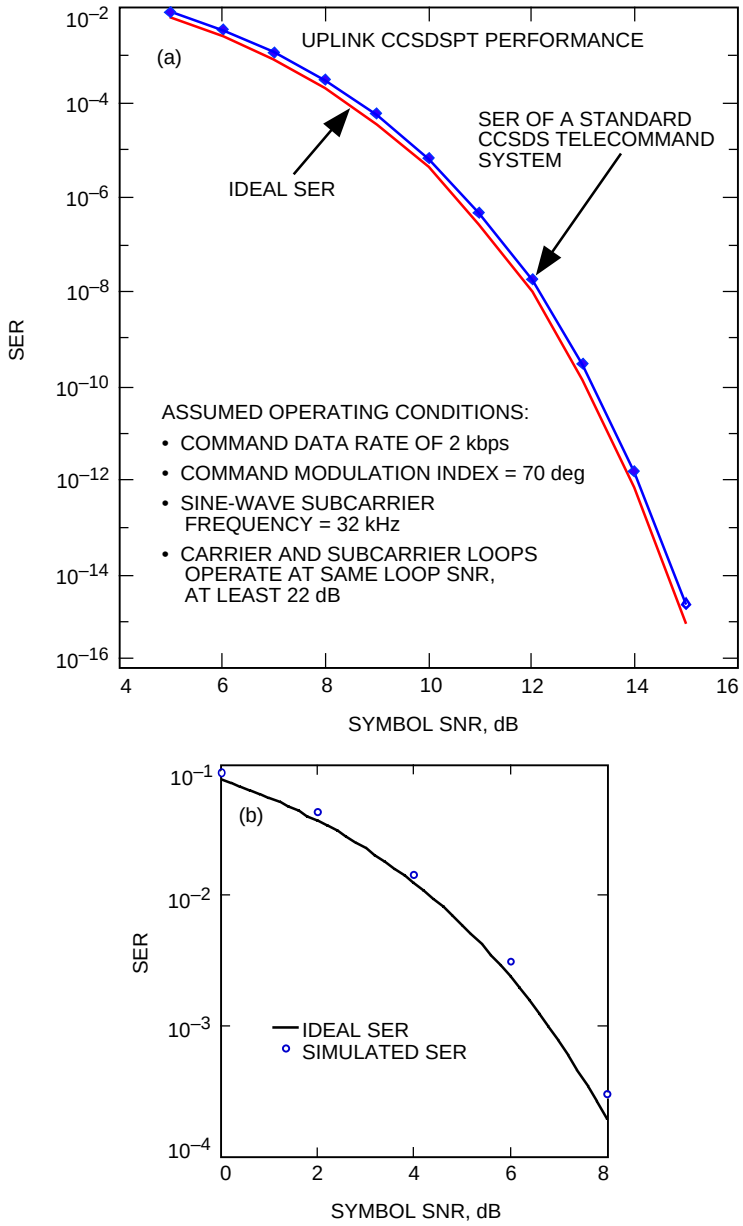

Fig. 6. Performance of system option no. 1: (a) the SER for a standard CCSDS telecommand system and (2) the simulated SER for a typical SFDMA telemetry system.

The downlink system performance for this proposed system can be worse than the current standard, single-user S/C system, depending on the available bandwidth, the downlink data rate, the Doppler profile, and the number of users in the band. The reason for this performance degradation is the Costas loop that was used instead of the PLL and the interchannel interference when the available spectrum is crowded with large numbers of high-rate data. Part of the interchannel interference problem can be alleviated by the insertion of sufficient guard band between adjacent signals, which should cover the maximum two-way Doppler offset when two S/C occupying adjacent bands are moving in the opposite direction. However, the PCM/PSK/PM signal modulated with a square-wave subcarrier as shown in Eq. (2) has an infinite number of data-bearing subcarrier harmonics at $(2k+1)f_{sc}$ that are slowly decaying

as the order increases. This inherent characteristic makes a certain degree of overlapping at higher-order subcarrier harmonics inevitable, no matter how far away the subcarriers are separated, unless the infinite number of subcarrier harmonics can be truncated by some means. Utilizing a bandpass filter on each S/C to remove higher-order subcarrier harmonics is a straightforward but, unfortunately, unfeasible answer to this because of the complexity of implementing a high-quality filter circuit for each S/C telemetry modulator. Passing the modulated subcarrier through a lowpass filter before putting it on the carrier is another way to limit higher-order subcarrier harmonics; however, it requires modification of the current S/C telemetry modulator design by adding such a lowpass filter. Using an alternative modulation, e.g., the PCM/PM/biphase modulation, is another answer. However, the fact that the biphase data need to be directly put on the carrier limits the use of this modulation to only one of the supported S/C. For the rest of the users, a subcarrier is still needed to be used for each of them. Hence, in order to maximize bandwidth efficiency to accommodate as many S/C as possible and to minimize the loss for each S/C, careful spectral utilization planning is very important.

An example is given here to show the number of S/C that can be packed by assuming available bandwidths of 3, 10, and 30 MHz for the SAML downlink, with the phase modulator in the current S/C transponder, whose passband is 30-MHz (two-sided) wide. First, let us assume that all S/C are transmitting at a data rate of 20 kbps and a guard band of 500 kHz is used.[4] For this example, one S/C will utilize PCM/PM/biphase modulation and the rest PCM/PSK/PM with square-wave subcarrier. The current telemetry modulator on board S/C supports subcarrier frequencies from 22.5 to 2880 kHz, with a factor of 2 increment. Taking into account the guard band and five data nulls for all modulations, the first subcarrier frequency, f_{sc1}, should be at 720 kHz. It can be shown that if the second and third subcarrier frequencies are selected such that $f_{sc2} = 2f_{sc1} = 1440$ kHz and $f_{sc3} = 4f_{sc1} = 2880$ kHz, none of the subcarrier harmonics within the 15-MHz one-sided bandwidth will overlap with the others, and the spacing between harmonics meets the guard band requirement. Table 1 shows the resulting center frequencies of each subcarrier's harmonics within the 15-MHz one-sided bandwidth. Based on this table, if the available two-sided bandwidth is 3 MHz, only one subcarrier at f_{sc1} can be used. (The one at f_{sc2} will not have enough guard band around it.) There is a 0.91-dB loss associated with this signal since only its first harmonic is available for signal detection. If the available two-sided bandwidth is increased to 10 MHz, then three harmonics of the first subcarrier at f_{sc1}, two harmonics of the second subcarrier at f_{sc2}, and one harmonic of the third subcarrier at f_{sc3} can be used. The maximum loss (0.91 dB) in signal power occurs on the third subcarrier. In this case, it is possible to pack one more spacecraft but at the expense of some degradation due to interchannel interference. For instance, a fourth S/C subcarrier can be put at 2160 kHz, which is the center frequency of the first S/C subcarrier's third harmonic, $3f_{sc1}$. The impact of the third subcarrier harmonic, which is 9.5-dB weaker than the first harmonic, on the first harmonic of the fourth S/C subcarrier is minimal (less than 0.1 dB). Note that this newly introduced S/C can have only one harmonic in the available bandwidth. Table 2 shows the number of users that can be supported for a 3-, 10-, or 30-MHz bandwidth and the maximum signal power loss incurred for any user. For a 30-MHz available two-sided bandwidth, the same number of users (up to five) can be supported as for the 10-MHz case, but with a smaller loss in each signal since more subcarrier harmonics can be accommodated. Note that the user using the 2160-kHz subcarrier has both of its first and third harmonics overlapped with the third and ninth harmonics of the user using the subcarrier at f_{sc1}.

A computer simulation was set up to investigate the spectral overlap effect when the downlink signals are not band limited. In this simulation, a typical SAML downlink scenario involving two Mars orbiters, each with a data rate of 20 kbps, was considered. One of the S/C had its telemetry biphase modulated directly on the fully suppressed carrier (PCM/PM/biphase with a 90-deg modulation index) and the other had BPSK-modulated telemetry on a square-wave subcarrier (PCM/PSK/PM) with a frequency of

[4] The guard band is determined from the maximum two-way Doppler offset that can be expected when two S/C occupying adjacent bands are moving in the opposite direction, plus a 25-percent margin.

Table 1. The center frequencies of subcarrier harmonics within the 15-MHz one-sided bandwidth for three subcarrier frequencies (f_{sc1} = 720 kHz, f_{sc2} = 1440 kHz, and f_{sc3} = 2880 kHz) used for SFDMA downlink.

No. of subcarrier harmonics	Subcarrier no. 1, kHz	Subcarrier no. 2, kHz	Subcarrier no. 3, kHz
1	720	1440	2880
2	2160	4320	8640
3	3600	7200	14,400
4	5040	10,080	—
5	6480	12,960	—
6	7920	—	—
7	9360	—	—
8	10,800	—	—
9	12,240	—	—
10	13,680	—	—

Table 2. SFDMA downlink performance example (note that both of the five-user cases have interchannel interference that gives slightly higher loss, represented as a "+").

Bandwidth, MHz	Maximum user loss, dB	No. of users
3	0.91	2
10	0.45	3
	0.91	4
	0.91^{+}	5
30	0.18	3
	0.30	4
	0.30^{+}	5

220 kHz.[5] The ground receiver was operated under normal tracking-mode conditions with a loop SNR for each of the carrier, subcarrier, and symbol synchronization loops higher than 18 dB. The simulated SER performance for the S/C with PCM/PSK/PM modulation is shown in Fig. 6(b), indicating an approximate 0.3-dB bit SNR degradation. It is expected that, under the same operating conditions, the SER for the other S/C will have similar degradation.

III. Description of System Option No. 2

The proposed system option no. 2 uses subcarrier frequency division multiplexing (SFDM) and CCSDSPT on the uplink and SFDMA on the downlink. Since SFDMA has already been described

[5] The worst Doppler effect was assumed and, therefore, no guard band was left between these two downlink signals to mimic the worst-case scenario. With the subcarrier at 220 kHz, the first three side lobes of the biphase-modulated signal will not overlap with the main lobe and the first four side lobes of the first subcarrier harmonic from the BPSK-modulated signal.

in Section II, this section only focuses on the hybrid SFDM and CCSDSPT on the uplink. Figure 7(a) depicts a simplified block diagram for this proposed uplink system architecture.

The main feature of this option is the increase of the uplink throughput by a factor of two (when using two subcarriers) as compared to option no. 1. As proposed in this option, the telecommands for all S/C are separated into two command data groups, with each group formatted as a CCSDS packetized telecommand stream and then phase-shift keyed on two different sine-wave subcarriers. The sum of these two subcarrier modulated signals is then phase modulated onto the RF carrier with different modulation indices [see Fig. 7(a)]. The uplink signal can be described mathematically as

$$S_u(t) = \sqrt{2P_u}\sin(2\pi f_u t + m_{u_1} d_{u_1}(t)\sin(2\pi f_{sc_1} t) + m_{u_2} d_{u_2}(t)\sin(2\pi f_{sc_2} t)) \tag{7}$$

where P_u is the uplink power; f_u denotes the uplink carrier frequency; and m_{u_i}, $d_{u_i}(t)$, and f_{sc_i} for $i = 1$ and 2 are the command data modulation index, the NRZ telecommand data, and the telecommand subcarrier frequency for the ith command data group, respectively. Expanding Eq. (7) yields [10]

$$\begin{aligned} S_u(t) = \sqrt{2P_u}\sin(2\pi f_u t)\{&J_0(m_{u_1})J_0(m_{u_2}) + O_1(nf_{sc_1}, mf_{sc_2}) \\ &- d_{u_1}(t)d_{u_2}(t)\sum_{n:odd}^{\infty} 2J_n(m_{u_1})\sin(2\pi n f_{sc_1} t)\sum_{m:odd}^{\infty} 2J_m(m_{u_2})\sin(2\pi m f_{sc_2} t)\} \\ &+ \sqrt{2P_u}\cos(2\pi f_u t)\{2d_{u_1}(t)J_1(m_{u_1})J_0(m_{u_2})\sin(2\pi f_{sc_1} t) + O_2(nf_{sc_1}, mf_{sc_2}) \\ &+ 2d_{u_2}(t)J_0(m_{u_1})J_1(m_{u_2})\sin(2\pi f_{sc_2} t) + O_3(nf_{sc_1}, mf_{sc_2})\} \end{aligned} \tag{8}$$

where $O_1(.,.)$, $O_2(.,.)$, and $O_3(.,.)$ are cross-modulation terms that produce interference and can be found in [10]. The spectrum of this signal is shown in Fig. 7(b).

Basically, this proposed option has all the limitations system option no. 1 has. Moreover, each S/C CDU is now required to be able to track any one of the two different subcarriers, and it is now faced with potential interchannel interference and cross-modulation interference in the uplink.

A. Interchannel and Cross-Modulation in the Uplink

Since there is only one uplink carrier being transmitted and it is assumed that there is no intermodulation caused by the ground station power amplifier, e.g., a traveling-wave tube (TWT) amplifier or the klystron power amplifier employed by the DSN, operated in the saturation mode [11], one is concerned only with the cross-modulation components produced by the nonlinearity in the phase modulation of two sine-wave subcarriers onto the same carrier [see Eq. (8)]. In order to minimize the cross-modulation interference effects, the uplink subcarrier frequencies, the command modulation indices, and the S/C receiver front-end bandpass filter parameters have to be chosen properly.

B. Uplink Performance of System Option No. 2

The uplink symbol error rate (SER) performance is at least 3-dB worse than that of option no. 1 since the uplink power is split to support simultaneously two command data streams at twice the data throughput as compared to option no. 1. Additionally, by assuming the system is properly designed, the symbol SNR loss due to cross-modulation interference and bandpass filtering can be reduced to between 0.2 and 0.5 dB. This number was calculated based on a filtering loss of 0.2 dB and a fixed but lower symbol SNR for both channels, and it will be used only as a first-order approximation for the system performance associated with this architecture. The real loss is expected to be worse than this.

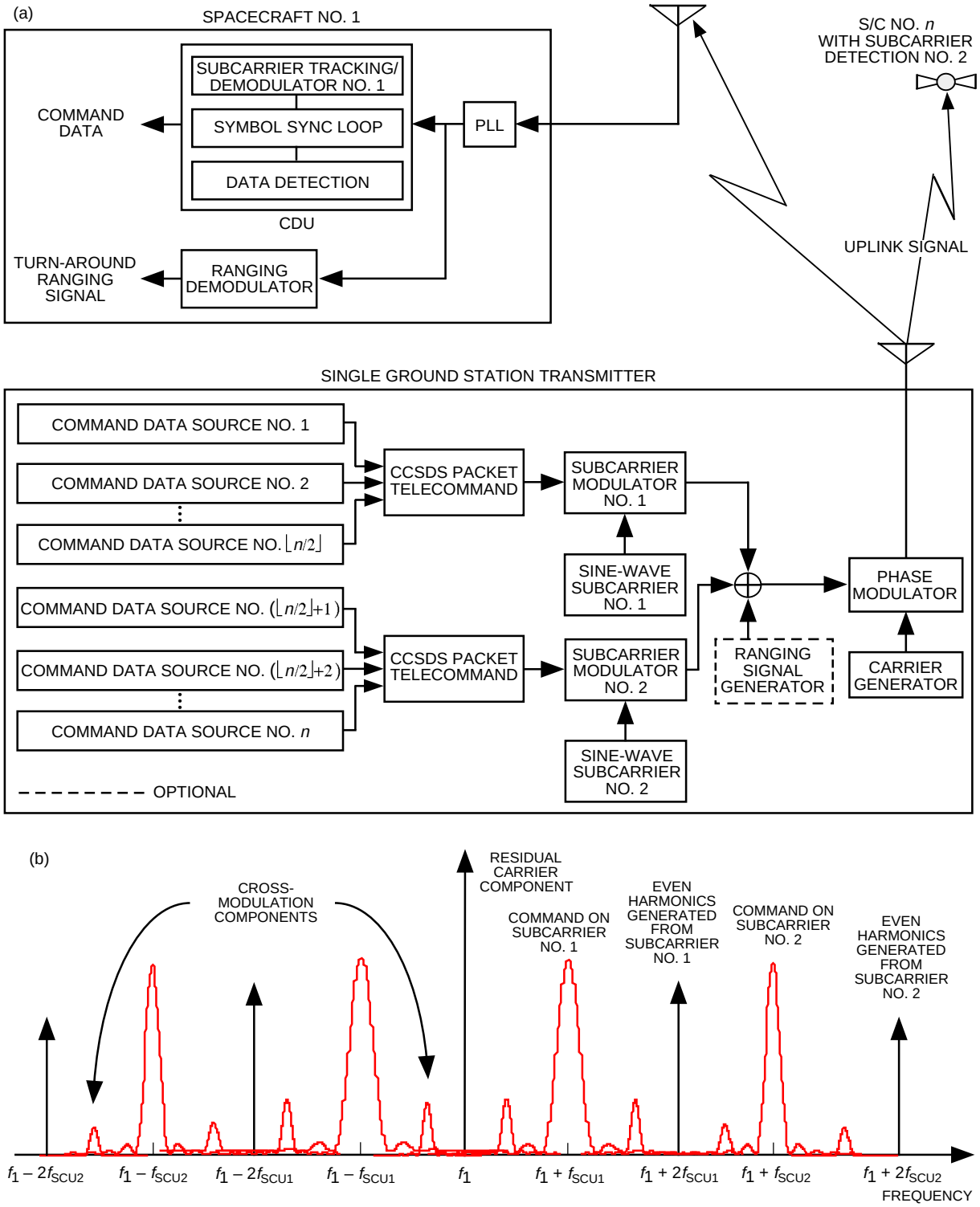

Fig. 7. System option no. 2: (a) a simplified block diagram for the SFDM uplink system and (b) the spectrum of the uplink signal without ranging signal.

IV. Description of System Option No. 3

The proposed system option no. 3 employs CCSDSPT on the uplink and CFDMA with an adjustable turnaround frequency ratio on the downlink. Since CCSDSPT has already been described in Section II, this section describes only CFDMA with an adjustable turnaround frequency ratio on the downlink. Figure 8(a) depicts a simplified block diagram for this proposed downlink system architecture.

For this option, the downlink signals are separated by using different downlink RF carrier frequencies. Since only one RF uplink carrier frequency is used on the uplink, various downlink RF carrier frequencies are generated by employing an adjustable transponder turnaround frequency ratio. The current recommended coherent turnaround frequency ratios (TFRs) are fixed at 240/221 for a 2-GHz band (S-band) and 880/749 for an 8-GHz band (X-band). To generate different downlink RF carrier frequencies for n different S/C, it is necessary to vary the coherent TFR in such a way that the downlinks are coherent with the uplink frequency f_u, with sufficient frequency separation to avoid spectral overlap among the S/C when Doppler shift is present. A standard downlink signal for each S/C employing PCM/PSK/PM with a square-wave modulation technique [5] can be used with this option, which renders the downlink signal as follows:

$$S_{d_i}(t) = \sqrt{2P_{d_i}} \sin(2\pi R_i f_u t + m_{d_i} d_i(t) Sq(2\pi f_{sc_i} t)) \tag{9}$$

where P_{d_i} is the downlink power, m_{d_i} denotes the downlink command modulation index for the ith S/C that is less than $\pi/2$, R_i denotes the ith coherent turnaround ratio, $d_i(t)$ is the NRZ telemetry data from the ith S/C, $Sq(\cdot)$ denotes the square-wave telemetry subcarrier, and f_{sc_i} is the subcarrier frequency of the ith S/C. The spectrum plot for Eq. (9) is shown in Fig. 8(b). Note that the subcarrier frequency for each S/C is not necessarily different from the others since the separation between downlinks in this option is mainly provided by sufficiently separated carrier frequencies. Nevertheless, using different subcarrier frequencies here can help to accommodate more low-rate S/C such that some of them can share a carrier without increasing the demand for new TFRs. For missions with high data rates, the CCSDS recommends that the downlink signals employ a PCM/PM modulation technique without a subcarrier, which is given by

$$S_{d_i}(t) = \sqrt{2P_{d_i}} \sin(2\pi R_i f_u t + m_{d_i} d_i(t)) \tag{10}$$

where, as above, $d_i(t)$ is the telemetry data from the ith S/C. Currently, a biphase data format is being considered for PCM/PM [13], resulting in PCM/PM/biphase modulation that can be treated as a special case of PCM/PSK/PM with a square-wave subcarrier at the data rate and a 90-deg modulation index.

Since the downlink signal is modulated on different residual RF carrier frequencies, this technique provides the best system in terms of SER. But to select various coherent downlink frequencies or various coherent TFRs for a deep-space transponder is a challenging task [14]. Due to many different constraints, the number of coherent TFRs available is finite and, once the TFR is implemented in the S/C transponder, it will be fixed for that particular mission. Therefore, mass production of several S/C transponders is not available with this technique. Since the multiple downlink signals are coherent with a single uplink signal, one has to consider the S/C receiver and the S/C exciter together. The feasibility of implementing different TFRs with the current available deep-space transponders (DSTs), namely, the Cassini DST, the Small DST, and the Tiny DST, has been investigated. It was found that both the Cassini and Small DSTs require modifying the S/C receiver circuitry of each transponder individually to have different turnaround ratios. Only the Tiny DST, currently in its design phase, is suitable for generating different downlink frequencies without modifying the transponder individually. Figure 9 shows the simplified Tiny DST architecture, which outlines how the coherent X-band downlink carrier is generated from the received uplink carrier frequency. The received uplink frequency is downconverted to 13.5F1 by mixing it with 735.5F1.

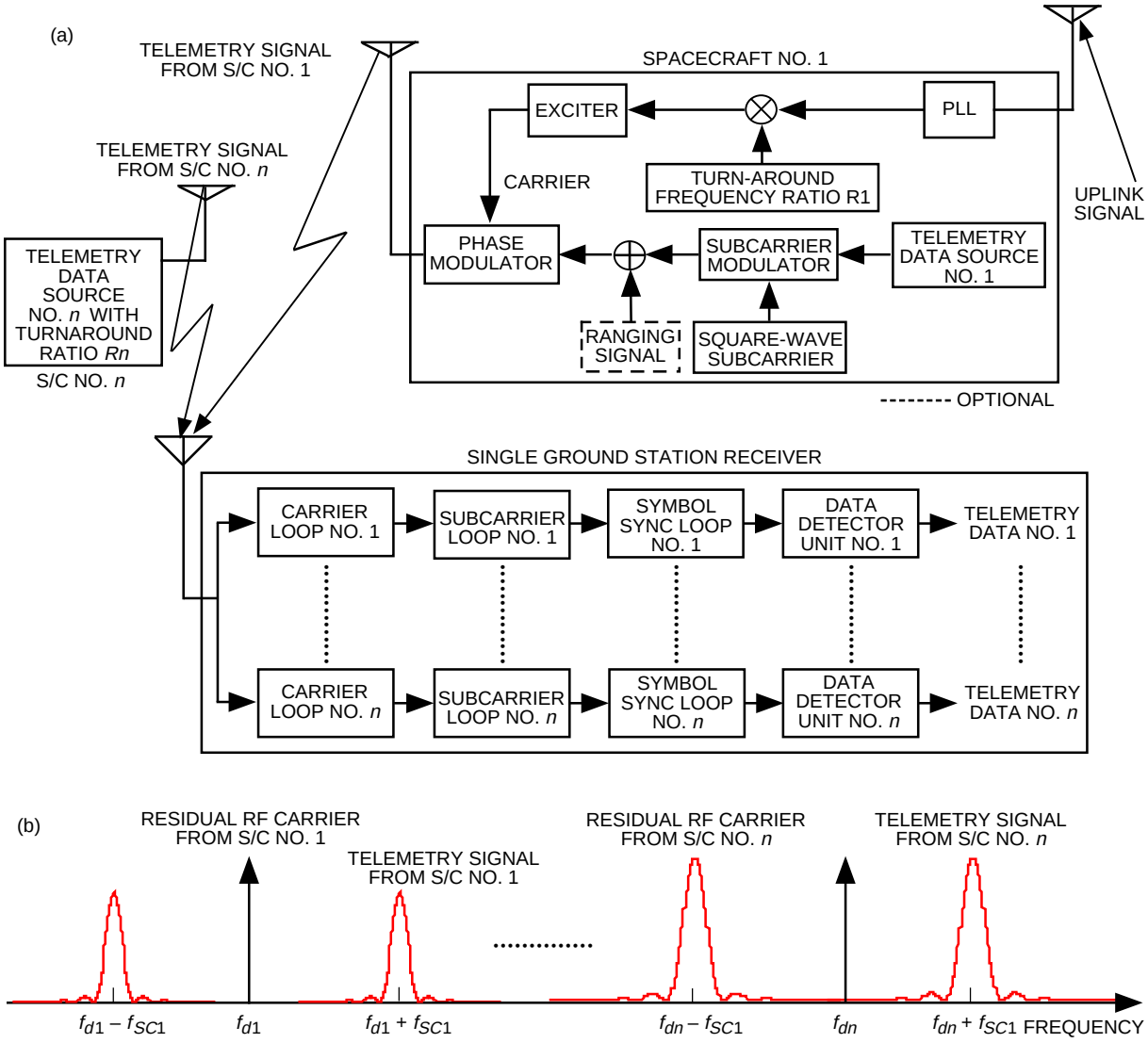

Fig. 8. System option no. 3: (a) a simplified block diagram of the CFDMA downlink system architecture with adjustable turn-around frequency ratio and (b) the spectrum of the downlink signal without ranging signal.

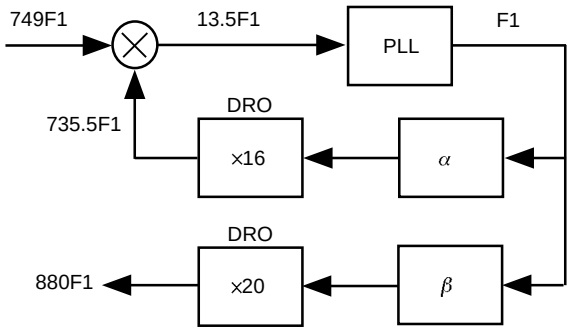

Fig. 9. The Tiny Deep-Space Transponder architecture.

The receiver PLL estimates the channel frequency F1. This estimate is used in a frequency synthesizer [that includes the receiver numerically controlled oscillator (NCO)] to generate a reference frequency of 45.96875F1 ($\alpha = 45.96875$). This reference output frequency is multiplied up by 16 in a dielectric resonant oscillator (DRO) loop to generate the 735.5F1 frequency that closes the receiver loop.

The exciter uses the same channel frequency estimate F1 to generate the coherent downlink carrier frequency. In the exciter, a frequency synthesizer (that includes the exciter NCO) generates a reference frequency of 44F1 ($\beta = 44$). This reference frequency is multiplied up by 20 in a DRO loop to generate the downlink 880F1 frequency.

Note that the Tiny DST architecture allows us to set the β factor to a different value to obtain a different downlink frequency without any modifications to the receiver loop design. However, to obtain downlink carriers that are separated more than 10 MHz requires that different exciter implementations be used in different transponders. If all the transponders use the same exciter implementation, the number and separation of downlink carriers are limited by the tunability ranges of the $\times 20$ DRO loop and of the reference frequency synthesizer. The current Tiny DST exciter design can accommodate three downlink carrier frequencies with about a 3-MHz separation between them, as shown in Table 3.[6] This table includes the frequencies for the turnaround ratios of 879.67/749, 880/749, and 880.33/749 that can be selected by choosing the β factors of 43.9835, 44.0000, and 44.0165, respectively. The Tiny DST design will be using frequencies for channel 19 operation.

Table 3. X-band uplink and downlink frequencies.

Channel	F1, MHz	Uplink	Downlink		
		749F1, MHz	879.67F1, MHz	880F1, MHz	880.33F1, MHz
14	9.5625	7162.31	8411.84	8415.00	8418.16
19	9.5709	7168.09	8418.63	8421.79	8424.95

Table 4 summarizes the desired transponder features for SAML support. These features are required for various reasons: a variable turnaround ratio for the CFDMA/ATFR option; a variable downlink subcarrier frequency for SFDMA; a variable uplink subcarrier frequency and data rate for SFDM; and S/C frequency-sweeping acquisition for total independent uplink acquisition among all S/C.

With the advance in digital frequency synthesizer technology, it is possible to build a simple lightweight variable TFR digital transponder that meets stringent deep-space requirements on frequency stability, spurious emission, and exciter bandwidth. To further reduce the cost and weight of the transponder, one can combine the RF phase extraction and digitization in one unit such that the second IF portion can be eliminated [15].

Performance of System Option No. 3

The uplink SER performance for this system architecture is identical to option no. 1, i.e., identical to the performance of the standard single S/C system. Since the telemetry is modulated on different carriers,

[6] The 3-MHz separation is required when a pair of turnaround ranging tones that are 1-MHz away from the carrier are used. It can be further reduced, say to a 1-MHz separation for 20-kbps PCM/PM/biphase-modulated telemetry signals and a guard band of 500 kHz, if no turnaround ranging signal is required.

Table 4. Key transponder features for SAML support.

SAML desirable features	Cassini DST	Small DST	Tiny DST
Variable turnaround ratio	No	No	Yes
Variable downlink, Subcarrier frequency	No	Yes 800 Hz–12 MHz, 0.7-Hz steps	Yes 0–4 MHz, continuous
Variable uplink subcarrier, Frequency and data rate	No 16-kHz subcarrier, data rate < 2 kbps	No 16-kHz subcarrier, data rate < 2 kbps	Yes Fully programmable
S/C initiated frequency sweeping acquisition	No	Maybe	Yes

the downlink SER performance for this architecture is also identical to the standard PCM/PSK/PM system for the single S/C case, which can be found in Fig. 5(a) and shows the bit SNR degradation to be about 0.2 dB under normal operating conditions.

V. Description of System Option No. 4

The proposed system option no. 4 employs CCSDSPT on the uplink and a code division multiple access (CDMA) scheme on the downlink. The uplink system architecture here is identical to the one proposed as option no. 1, and the spectrum of the uplink signal can be found in Fig. 2(c). Hence, this section only deals with the downlink. Figure 10(a) depicts the simplified block diagram for the proposed downlink system architecture.

To separate the downlink channels, the proposed system uses CDMA architecture in which each S/C uses its preassigned pseudorandom noise (PN) code sequence directly modulated on the telemetry data, and then phase modulated on a downlink RF carrier at a frequency common among all S/C. The received downlink signal can be modeled as [12,16]

$$S_d(t) = \sum_{i=1}^{N} \sqrt{2P_{d_i}} \cos(2\pi f_d t + 2\pi f_{d_i} t + m_{d_i} c_i(t-\tau_i) d_i(t-\tau_i) + \theta_i) \tag{11}$$

where N is the number of S/C; f_d is the downlink frequency; and P_{d_i}, $c_i(t)$, and $d_i(t)$ are the received signal power, PN code sequence, and telemetry data for the ith spacecraft, respectively. Also indicated in this equation are the Doppler shift f_{d_i}, the time delay τ_i, the random phase θ_i, and the telemetry modulation index m_{d_i} associated with the ith S/C. The spectrum of this downlink signal with fully suppressed carrier (i.e., $m_{d_i} = \pi/2$, for all i) is illustrated in Fig. 10(b).

As shown in Fig. 10(a), the received downlink signal is fed through a bank of receivers, each equipped with one of the PN code generators (part of the PN demodulator) used in a specific S/C. With a properly designed code set, the cross-correlation between different PN code sequences can be minimized so that the downlink channels are effectively separated. Also, the PN sequences should possess very good autocorrelation property so that they can serve as ranging codes for each S/C. At the ground station receiver, a noncoherent code tracking loop, followed by a conventional carrier tracking loop, is used to provide chip-level synchronization, since the carrier phase reference is generally not available at a very low SNR. Once accurately synchronized, the PN code can be removed easily by multiplication with

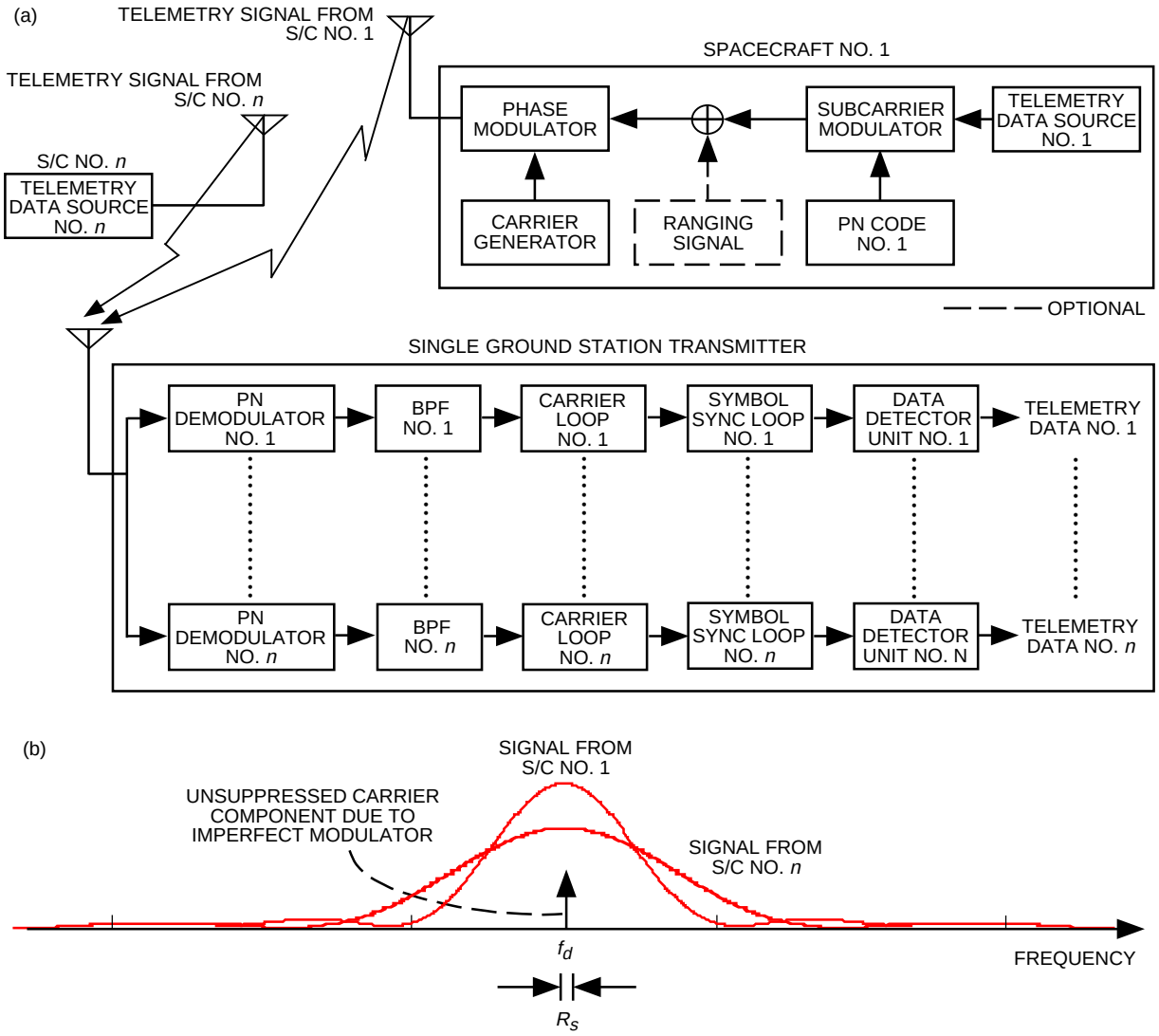

Fig. 10. System option no. 4: (a) a simplified block diagram of the CDMA downlink system architecture and (b) the spectrum of the downlink signal without ranging signal (where R_S is the telemetry symbol rate).

its replica, rendering a despread narrowband signal embedded in the wideband interference from other S/C sharing the same spectrum and background thermal noise [12,16].

The feasibility of CDMA technology has been demonstrated by a commercial mobile cellular system that is based on the North American DS-CDMA Digital Cellular System Standard (IS-95 standard) [17]. The CDMA chip rate is 1.2288 MHz and operates in the L-band (between 1.7 and 1.8 GHz). For the reverse link (from mobile users to the base station), the commercial CDMA system assigns to each user a unique period-$(2^{42}-1)$ long PN sequence to distinguish signals arriving from different mobile users. In addition, a pair of period-2^{15} short PN codes, distinguished for each cell by a specific time offset from a base code, is used to modulate the spread and scrambled user signal into a filtered offset quadrature phase shift keying (QPSK) format. According to IS-95, the reverse channel can accommodate up to 62 traffic channels in a cell. In order to alleviate the power dissimilarity due to different distances to the base station from each mobile user in a cell (the so-called near–far problem), the system has a two-way power control scheme implemented that can adjust the received power from each mobile user to within 1 dB.

The CDMA downlink option is similar to the reverse link of the commercial cellular system. However, in deep-space missions, we have channels that are more power limited than bandwidth limited. Also, a similar power regulation issue may need to be addressed because of different types of S/C antennas and data rates supported. Some issues and limitations related to the CDMA downlink can be identified as follows:

(1) PN code set design: This is required to (1) minimize interference among channels; (2) preserve reliable tracking; and (3) possibly provide accurate ranging measurement.

(2) Bandwidth efficiency: The question regarding bandwidth efficiency has to be answered properly here.

(3) Power regulation among all users: This is to avoid the power dissimilarity problem, which can cause severe performance degradation for S/C with a weaker signal.

(4) Doppler/Doppler rate effects on PN code acquisition/tracking: One-way Doppler and Doppler rate exist in this case, and their effects on PN code acquisition and tracking potentially may cause degradation, especially at a low SNR.

(5) Residual carrier tone for navigation: This may be needed to satisfy radio science requirements.

The use of this system requires modifications to both S/C and ground station hardware. The S/C transponder requires a PN code generator and PN code modulator, while in the ground station receiver, a PN code demodulator is required for telemetry data demodulation.

Performance of System Option No. 4

Again, the uplink system performance for this proposed option is identical to uplink system option no. 1. For the downlink, the performance of this system is limited by the number of user S/C. A numerical simulation was set up to mimic the downlink error performance. The results are plotted in Fig. 11. Figure 11(a) shows the bit SNR loss versus the spreading ratio for different numbers of active user S/C. With a larger number of users, the spreading ratio for each S/C has to be increased to overcome the stronger interference from other S/C. Also, the higher transmitting power from some or all S/C inevitably generates stronger interference to others. This can be shown in Fig. 11(b), in which the loss is plotted versus the spreading ratio for a lander with weaker transmitting power (20 and 30 dB lower) than that of two orbiters. The assumption of a common PN code chip rate among users is made here. It should be mentioned here that the selection of proper PN code sequences will play an important role in the design of spread spectrum communications systems [18,19]. Three families of binary PN codes favorable for deep-space communications, namely, the M-sequences, Gold sequences, and Kasami sequences, are discussed in Appendix D. The M-sequences are good for a small and limited number of users. Gold codes are selected for communications systems with a large number of users. Kasami codes are recommended for systems with a limited number of users [19].

VI. Description of System Option No. 5

The proposed system option no. 5 employs code division multiplexing (CDM) with Walsh–Hadamard (WH) codes on the uplink and code division multiple access (CDMA) for the downlink. Only the CDM uplink is described here since the CDMA downlink has already been described in option no. 4. Figure 12 (a) shows a simplified block diagram for this proposed uplink architecture. Figure 12(b) shows a set of regular length-8 WH codes used for this CDM uplink. The WH codes are well known for their zero cross-correlation when they are perfectly aligned [19–22]. Thus, if synchronization among all users can be maintained, the WH codes provide orthogonal channels for all S/C. The use of WH codes is well justified on the uplink because the transmitted data for each S/C can be synchronized

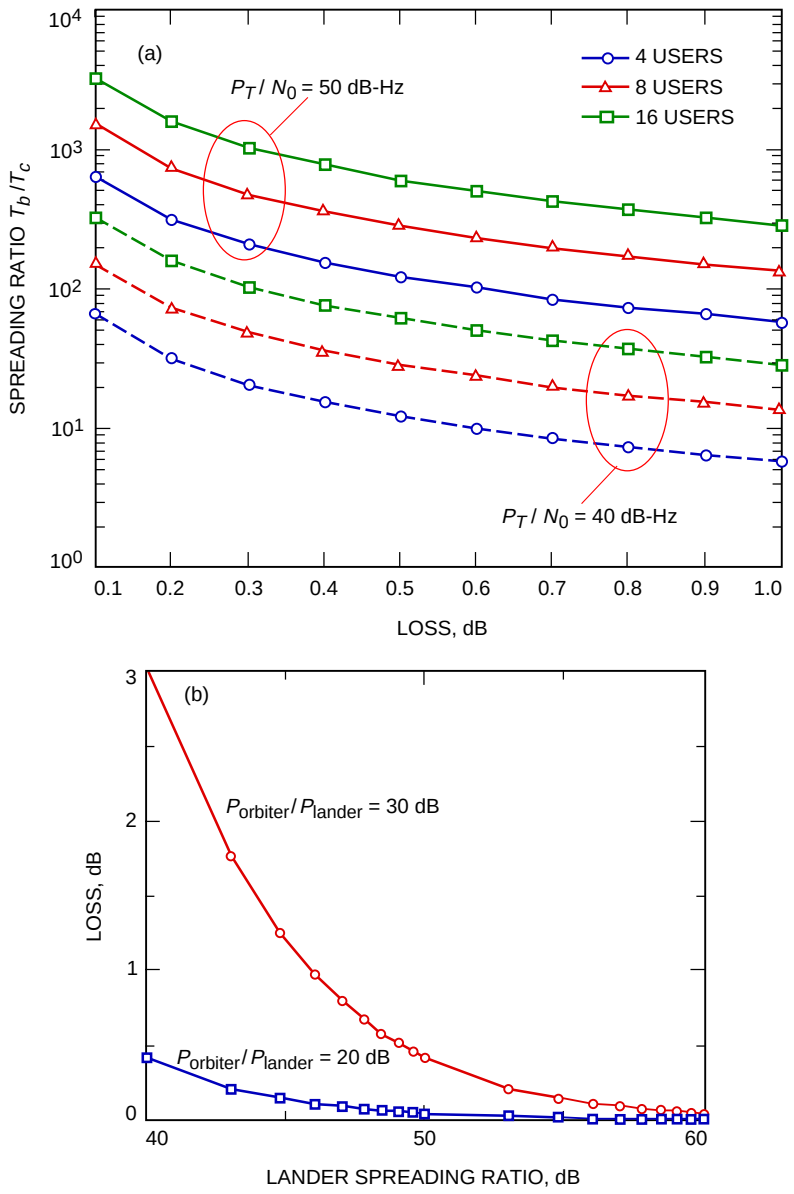

Fig. 11. Performance of system option no. 4: (a) loss versus the spreading ratio for spacecraft at a data rate of 20 kbps and (b) the lander spreading ratio versus loss in a three-user scenario (two orbiters and one lander).

to start at the same time. In the downlink, however, the starting time of data transmission for each S/C is completely random, and the use of WH codes is not applicable.

For the uplink, CDM has two important advantages over the CCSDSPT multiple-access scheme described in option no. 1. The first advantage is that the command data for CDM is transmitted simultaneously for all active S/C, spread both in time and frequency. The command data for CCSDSPT, in contrast, are disjoint in time and must be transmitted sequentially. If the uplink command data transmission is constrained in time, then the CDM scheme appears more attractive than CCSDSPT. The second advantage of CDM over CCSDSPT is that it can support different physical data rates. As a result, the

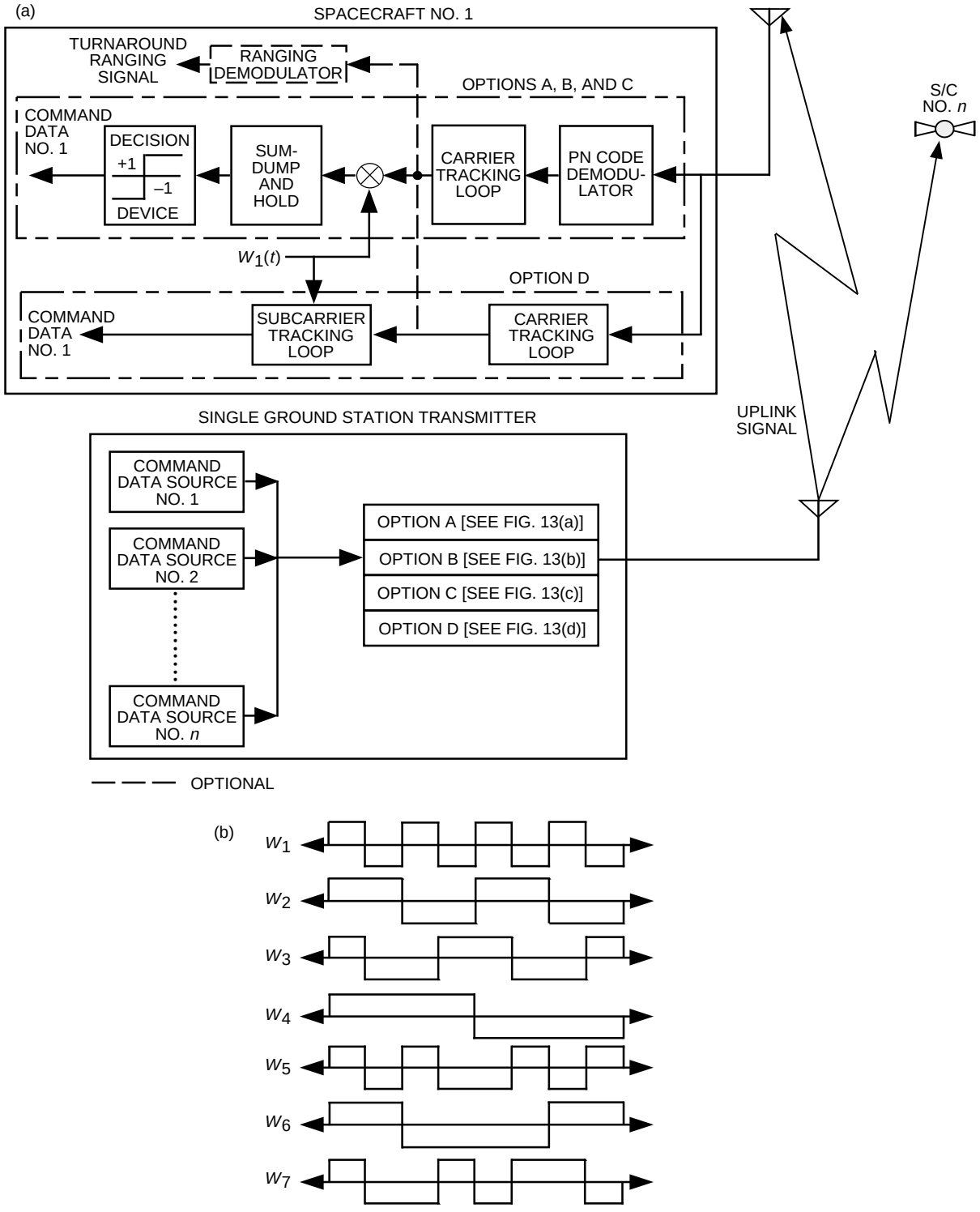

Fig. 12. System option no. 5: (a) a simplified block diagram for the CDM uplink system and (b) regular length-8 Walsh functions (W_0 = 1 is not included here).

command data rate specification for a lander and an orbiter can be different, which can simultaneously support both the orbiter (using an HGA for high-rate data) and lander (using an LGA for low-rate data) with a reasonable performance margin. The disadvantage of CDM over CCSDSPT is that modification to the present S/C hardware configuration is required. Four representative options of CDM are described in detail along with their corresponding advantages and limitations. The system structure variation of these four options stems from the trade-offs in two areas: (1) constant-envelope signal to achieve maximum power efficiency or multilevel signal to preserve orthogonality, and (2) simplicity in modification of the existing system.

A. Option A of CDM Uplink

Figure 13(a) shows a simplified block diagram for option A, where the ith command data source (CDS) output $d_i(t)$ is synchronously multiplied by the ith WH code waveform $W_i(t)$ such that each command data bit duration is aligned with the WH code duration. The output of the summer in Fig. 13(a) can be written as [18]

$$X(t) = A_0 W_0(t) + d_1(t)W_1(t) + \cdots + d_M(t)W_M(t) = A_0 + \sum_{i=1}^{M} d_i(t)W_i(t) \tag{12}$$

where $d_i(t)$ and $W_i(t)$ are, respectively, the command data and WH code waveform for the ith S/C, and M is the number of user S/C, which should be less than N, the number of WH code bits per command data bit. The output of the summer is then multiplied coherently by a PN code sequence, $c(t)$, with a chip rate equal to the WH code bit rate. Note that $W_0(t) = 1$ is a constant function that, after the

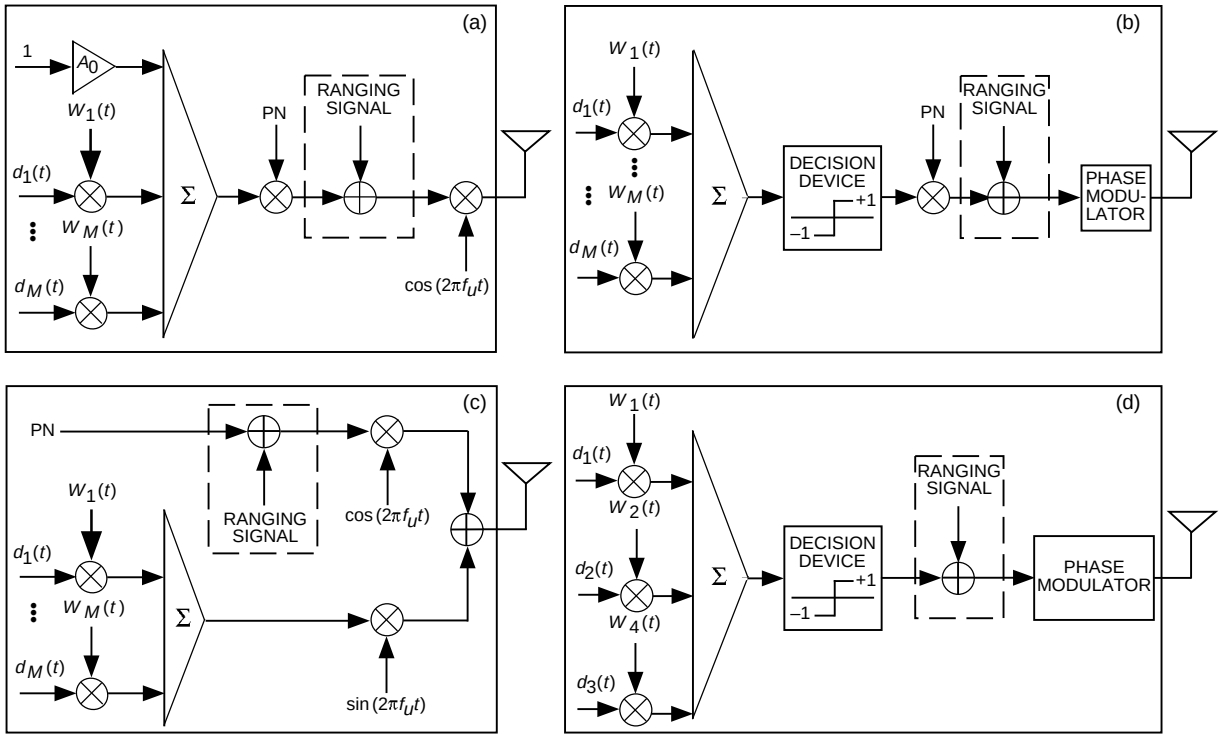

Fig. 13. The options for CDM using Walsh–Hadamard code: (a) option A, (b) option B, (c) option C, and (d) option D (an example of a three-user case).

multiplication with the PN code, generates an unmodulated PN code. The purpose of using a PN code here is to provide WH codeword synchronization for S/C receivers, by taking advantage of the unique auto-correlation characteristic of a PN code. The WH code itself has a poor auto-correlation property and, thus, is not able to be used alone for synchronization purposes. The constant signal A_0 in Eq. (12), which is typically larger than the amplitude of the other WH code modulated command data, becomes what is conventionally called the pilot tone [18] after being modulated by the PN code. Tracking of this stronger pilot tone signal by each S/C can provide important WH codeword synchronization, required for the removal of WH code modulation by the S/C receiver. The resulting multilevel signal is then amplitude modulated onto an RF carrier at frequency f_u, and modeled mathematically as

$$S_u(t) = \sqrt{2P_u}c(t)\overline{X(t)}\cos(2\pi f_u t) \tag{13}$$

where P_u is the average transmitted uplink power and $\overline{X(t)}$ is the normalized version of $X(t)$ in Eq. (12), such that its average power is unity. The key feature for this option is that the transmitted signal is amplitude modulated, unlike the traditional deep-space signal modulation format, which is phase modulated. Hence, significant back off in ground-station power amplifier operation is required here.

For the ith S/C shown in Fig. 12(a), the pilot sequence timing is determined before any carrier phase measurement or tracking is attempted. First a coarse acquisition must be performed to get the received and locally generated PN sequences aligned to within a chip. Since the carrier is not tracked, the coarse acquisition process must be noncoherent, normally requiring a squaring operation to measure energy. Once the pilot PN sequence timing has been established to within a chip, continuous tracking can be made using some noncoherent code tracking loop, such as a delay-locked loop. After chip synchronization, the carrier is tracked using a Costas loop and removed from the received RF signal. Afterwards, the ith S/C user coherently multiplies the demodulated baseband signal by the local reference $W_i(t)$, which is driven by the previously established pilot PN sequence timing, to obtain the data waveform $d_i(t)$.

Option A of CDM is similar to the forward link (from the base station to the mobile users) in the commercial CDMA cellular system, in which Walsh codes of length 64 are used for a cell: one pilot channel used for acquisition/tracking and received signal strength indication; one synchronization channel for system timing and other system-related messages; and 62 channels for paging/traffic. The pilot signal level is typically from 4- to 6-dB higher than each of the other 62 traffic channel signals. The cellular system supports data rates of 1.2, 2.4, 4.8, or 9.6 kbits/s with a constant energy per bit. Each forward traffic channel uses a unique long PN sequence of period-$(2^{42}-1)$ to scramble the coded symbol, which is at a fixed symbol rate of 19.2 ksymbols/s. After WH code modulation, the modulated symbol rate becomes 1.2288 Msymbols/s, which is equal to the PN chip rate. A pair of period-2^{15} short PN codes, distinguished for each cell by a time offset from a base code, are then used to modulate the composite signal into a filtered QPSK format. Moreover, the transmitter for the base station operates in the linear region.

The advantages and limitations of option A are described below. The inherent advantages identified for this option are as follows:

(1) Pilot tone: This is essential to improve acquisition and tracking of PN code.

(2) WH codes: All users are orthogonal to each other.

(3) Bandwidth expansion: Since PN chip rate and WH code bit rate are identical, there is no additional bandwidth expansion.

However, the number of users that can be supported in this option is limited by the ground-station power amplifier since the power amplifier for a multilevel signal must operate in the linear region. Significant power back off, required to accommodate such a multilevel signal, will greatly reduce the power efficiency and render a lower received power level on the S/C.

SER performance for Option A

Without considering the PN code tracking performance, the SER performance of option A will be similar to the ideal BPSK case, except that there is a symbol SNR reduction due to a portion of power allocated to the pilot signal. However, when compared with the available transmitting power when the amplifier is operated at saturation, the assumption that the amplifier operates in the linear region to transmit an AM signal implies an additional symbol SNR loss because of the required power back off from saturation, which will render further performance degradation, since the available transmitting power is significantly reduced. This will be discussed together with option C in Appendix E, and an example of a required power back-off comparison is given in Table 5, where the peak-to-average power variation for the multilevel input signal to the power amplifier in options A and C is given as a function of the number of users, by assuming a pilot tone consuming a percentage (α) of the average transmitted power.

Table 5. The peak-to-average power variation of the multilevel input signal to the power amplifier in options A and C versus the number of users with either 50 percent or 30 percent of the average transmitted power allocated to the pilot signal (the 50 and 30 percent power reductions account for an additional 3.01-dB and 1.55-dB loss, respectively).

No. of users	Peak-to-average power variation ($\alpha = 50\%$)		Peak-to-average power variation ($\alpha = 30\%$)	
	Option A, dB	Option C, dB	Option A, dB	Option C, dB
1	3.01	0.00	2.83	0.00
2	4.65	1.76	4.77	2.30
3	5.72	3.01	6.01	3.80
4	6.53	3.98	6.93	4.91
5	7.19	4.77	7.67	5.80
6	7.74	5.44	8.29	6.53
7	8.23	6.02	8.82	7.16

B. Option B of CDM Uplink

Figure 13(b) illustrates option B for the CDM scheme, using majority logic multiplexing [30] where the command data and WH code products are summed and then hard limited. One of the two major advantages of this scheme is that the resulting binary signal at the hard-limiter output is a constant envelope and enables phase modulation so that the power amplifier can operate at saturation, providing maximum power efficiency [11]. This is not feasible for the multilevel signal in option A because of the potential for poor error performance of an M-ary phase shift keying (MPSK) signal (when M is large) and the difficulty of designing an MPSK receiver for a dynamically changing number of users. The other advantage (see Appendix F) is that the transmitted data are redundantly encoded so that some error correction capability is provided, especially when the system is not fully loaded. However, unlike option A, where the WH codes ensure that all the users are mutually orthogonal, the use of the hard limiter destroys the orthogonality property and can cause ambiguity in some cases. The details of using the Walsh function for majority logic multiplexing are summarized in Appendix F. The hard-limiter output can be written as

$$Y(t) = sgn\left[d_1(t)W_1(t) + d_2(t)W_2(t) + ... + d_M(t)W_M(t)\right] = sgn\left[\sum_{i=1}^{M} d_i(t)W_i(t)\right] \tag{14}$$

where again $d_i(t)$ and $W_i(t)$ are the data and WH code waveform for the ith user, respectively, and $sgn(\cdot)$ denotes the signum function. The output is then multiplied by a PN sequence with period equal to one WH code bit. The PN code is needed here to determine the WH codeword timing. Note here that, for this option, the PN chip rate is not equal to the WH code bit rate; in fact the former is much larger than the latter. The binary signal is then phase modulated onto the RF carrier frequency, and the transmitted signal is given by

$$S_u(t) = \sqrt{2P_u}\cos(2\pi f_u t + mc(t)Y(t)) \tag{15}$$

where m denotes the modulation index.

For a fully suppressed carrier, the demodulation process on the S/C for option B is identical to that of option A, namely, noncoherent PN code tracking followed by carrier and WH code demodulation. If $m < \pi/2$, however, the residual carrier phase may be tracked by using a PLL before PN code acquisition and tracking, provided that the residual carrier tone is strong enough. This may be a desirable feature since the present S/C are configured to use coherent demodulation. In this case, for the ith S/C shown in Fig. 12(a), the PN code and carrier are first tracked, and then the demodulated signal is correlated with a local reference, $W_i(t)$, to obtain the data, $d_i(t)$.

The major advantage of this option over option A is that the ground-station power amplifier can now operate in saturation at all times because the transmitted signal is phase modulated with a constant amplitude modulation. The use of this option is constrained by three factors:

(1) Acquisition: Code acquisition and tracking can be difficult since no pilot tone is used.

(2) Bandwidth expansion: PN chip rate is much larger than WH code symbol rate.

(3) Number of users: This is limited by the majority logic multiplexing. Users are no longer orthogonal to each other after passing the composite signal through the hard limiter.

SER performance for Option B

Figure 14 shows the computer simulation results for the SER performance of this option, when the truncated length-7 WH functions are used and hard decision is made on each WH bit (see Appendix F). It is clear that the penalty paid for using a hard limiter at an SER of 10^{-5} for two to three users is 5.53 dB and is 8.8 dB for six to seven users, as compared with the ideal BPSK SER performance. Note that, for four and five users, redundant data streams can be used to keep the system fully loaded and, therefore, the SER performance in this case will be the same as that for six to seven users.

C. Option C of CDM Uplink

Option C, shown in Fig. 13(c), utilizes a quadrature multiplexing to put the data and PN code separately through the I channel and Q channel. In the I channel, the command data and WH code products are summed and then amplitude modulated onto the in-phase RF carrier. In the Q channel, the PN code waveform, which is used for WH codeword synchronization, is phase modulated onto the quadrature carrier. The I and Q channels are then summed and transmitted. The quadrature multiplexed signal becomes an unbalanced quadrature amplitude modulated (QAM) signal and, in general, is given by

$$S_u(t) = \sqrt{2\alpha P_u}\sin(2\pi f_u t + c(t)) + \sqrt{2(1-\alpha)P_u}\ \overline{Z(t)}\cos(2\pi f_u t) \tag{16}$$

where α is a percentage of average transmitting power P_u allocated to the pilot signal and $\overline{Z(t)}$ is the normalized version of

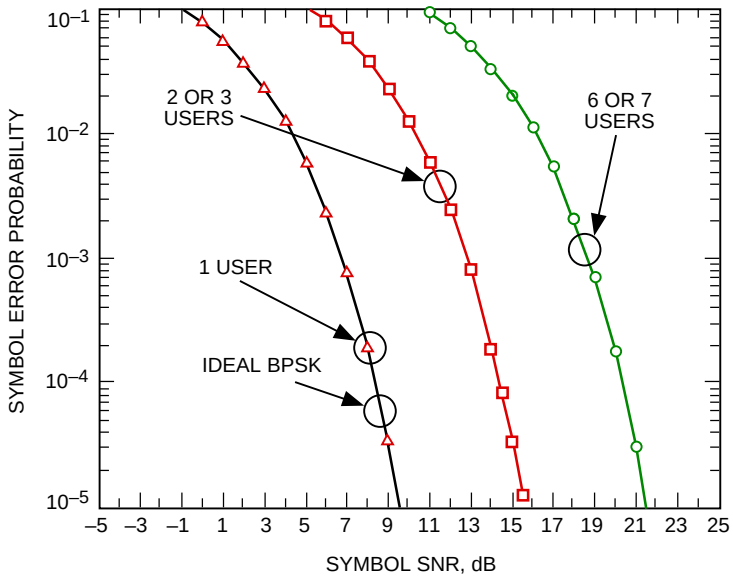

Fig. 14. Performance of a truncated Walsh–Hadamard function of size 7 for various users.

$$Z(t) = \sum_{i=1}^{M} d_i(t) W_i(t) \tag{17}$$

such that its average power is unity. This option is similar to option A, except that a QAM modulation is used here. It preserves the orthogonality among all users at the expense of not having a constant-envelope waveform. One of the major advantages over option A is that the PN pilot sequence can be easily acquired and tracked for WH codeword synchronization since it is on a separate (quadrature) channel. Moreover, the PN chip and WH code bit rates used here can be identical, which does not cause additional bandwidth expansion. Another advantage is that the peak-to-average power variation of the transmitted signal in this option is less than that in option A, which reduces the amount of power amplifier back off required for a nonconstant-envelop signal. The inherent problem of phase ambiguity associated with QPSK systems can be resolved by utilizing an offset quadrature phase-shift keying (OQPSK) modulation scheme [23] so that the receiver can determine which channel has the PN sequence and which has the data.

For signal demodulation on the S/C, option C is identical to option A but requires a QPSK carrier loop. For the ith S/C shown in Fig. 12(a), the PN code and the carrier in the quadrature channel are first tracked and then, for the ith user, the demodulated signal in the in-phase channel is correlated with a local reference, $W_i(t)$, to obtain the data, $d_i(t)$.

The major disadvantage for this option is that a QAM demodulator in the S/C transponder is required, which renders a complete redesign of the transponder. Note that a variation similar to option B can be realized by using a hard limiter on the multilevel signal.

SER performance for Option C

The SER performance of this option is similar to that of option A, except that the QAM signal requires a smaller amount of power amplifier back off here. This will be discussed together with option A in Appendix E, and an example of a required power back off comparison is given in Table 5.

D. Option D of CDM Uplink

Figure 13(d) illustrates option D, which is similar to option B but no PN sequence is used. For this option, the transmitted signal can be described mathematically as

$$S_u(t) = \sqrt{2P_u}\cos(2\pi f_u t + mY(t)) \tag{18}$$

where $Y(t)$ is defined in Eq. (14) and where WH codes are chosen from a subset of the WH codes consisting only of square-wave waveforms. For example, such a subset of regular length-8 WH codes has only W_1, W_2, and W_4, as shown in Fig. 12(b). These square-wave WH waveforms can be treated as square-wave subcarriers, which are modulated by data streams and then passed through the hard limiter. The key advantage of option D over option B is that, at the receiving end, a conventional subcarrier tracking loop can be used to track the square-wave WH waveforms and, after the removal of the subcarrier, data can be tracked by a conventional symbol-timing tracking loop without using majority logic demultiplexing, which requires the assistance of a PN code to establish WH codeword synchronization. Moreover, not using a PN code can greatly reduce the required modification to the current system, and no bandwidth expansion is incurred beyond that of options A and C. The key disadvantage of option D is that additional degradation is incurred in the subcarrier and the symbol-timing tracking loops, due to the presence of hard-limited square-wave subcarriers. Figures 15(a) and 15(b) respectively show the unnormalized and normalized subcarrier S-curves when each of the 16-kHz, 8-kHz, and 4-kHz square-wave subcarriers, modulated with independent data streams at 1 kHz, is tracked, the hard-limited composite waveform $Y(t)$ being the input to the subcarrier loop. The S-curve of the regular square-wave subcarrier is also included for reference. The slope of the S-curves was found by simulation to be 0.157. Moreover, Fig. 16 shows the loop SNR when each subcarrier embedded in the hard-limited composite waveform is tracked. Compared to the tracking performance of the regular subcarrier, the hard-limited multiple subcarriers incur an additional 7-dB loss in loop SNR. The degradation incurred in the symbol-timing tracking loop, such as the digital data-transition tracking loop (DTTL), needs further analysis.

Similar to option B, the major advantage of this option over option A is that the ground-station power amplifier can operate in saturation. Use of this option is constrained by the following:

(1) Number of users: This is still limited by the hard limiter. Users are no longer orthogonal to each other after passing through the hard-limiter.

(2) Phase jitter: An increase in phase jitter is incurred in the subcarrier and the symbol-timing tracking loops due to the hard-limited square-wave subcarriers.

SER performance for Option D

Without considering the subcarrier and symbol-timing tracking performance, this option suffers a penalty, similar to those in options B and C, for using WH-based majority logic multiplexing. For the three-user case, it is 5.53 dB at an SER of 10^{-5} as compared with the ideal BPSK SER performance. For each additional user beyond the three, WH codes of twice the length would be required. Serious synchronization problems are expected in this option because of the use of a hard limiter on a large number of users.

E. Comparison of CDM Options for System Option No. 5

Table 6 summarizes some key features for the various options proposed for system option no. 5. Of these four options, options A and C use amplitude-modulated (AM or QAM) signals, which requires that the power amplifier operate in the linear region and results in a reduction in output power level. On the other hand, options B and D use phase-modulated (PM) signals, which achieve the maximum power efficiency, at the expense, however, of SER performance degradation due to hard limiting the composite signal.

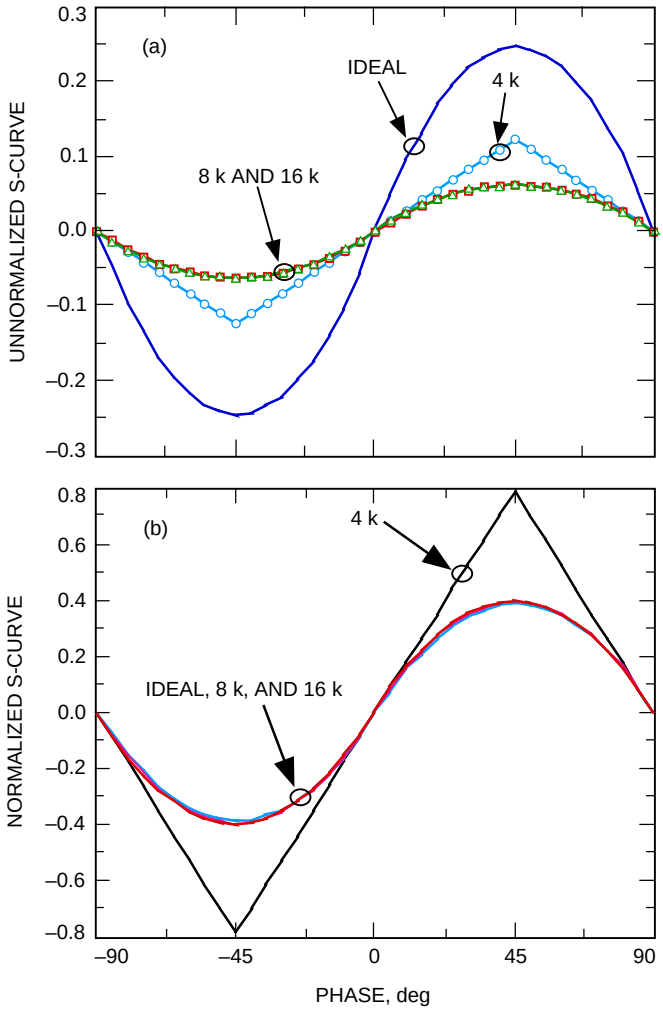

Fig. 15. S-curves for tracking 4-, 8-, and 16-kHz subcarriers: (a) unnormalized and (b) normalized.

The key question for options A and C is how much the power amplifier back off from saturation can be tolerated such that a reasonable uplink symbol SNR margin is still met. Figure 17 shows a typical input and output power relationship for the DSN klystron power amplifier. This curve shows the effects of AM–AM and AM–PM on the transmitted signal. The AM–PM curves determine the maximum carrier phase degradation that can be tolerated, which is defined as $[\cos^2(\text{phase})]_{dB}$. For example, if the maximum tolerable carrier degradation is 0.1 dB, then the maximum input power can be no greater than 18 dBm. If the maximum carrier degradation tolerable is relaxed to 0.5 dB, the maximum input power then becomes 21 dBm. Thus, it is clear the maximum input power is upper bounded by the amount of carrier degradation that can be tolerated.

The minimum input power that must be maintained, on the other hand, is determined by the link margin. For instance, the total received power on the uplink for the Mars mission was calculated to be about 48 dB-Hz. To support the maximum data rate of 2 kHz, the received symbol SNR becomes 15 dB. If the minimum symbol SNR that must be maintained is 10 dB, then the symbol SNR link margin becomes 5 dB (15 dB − 10 dB). Thus, as shown in Fig. 17, the minimum output power becomes 66 dBm, which corresponds to an input power of 14 dBm. Consequently, the input power variation is bounded by 4 dB and 7 dB for a carrier degradation of 0.1 dB and 0.5 dB, respectively.

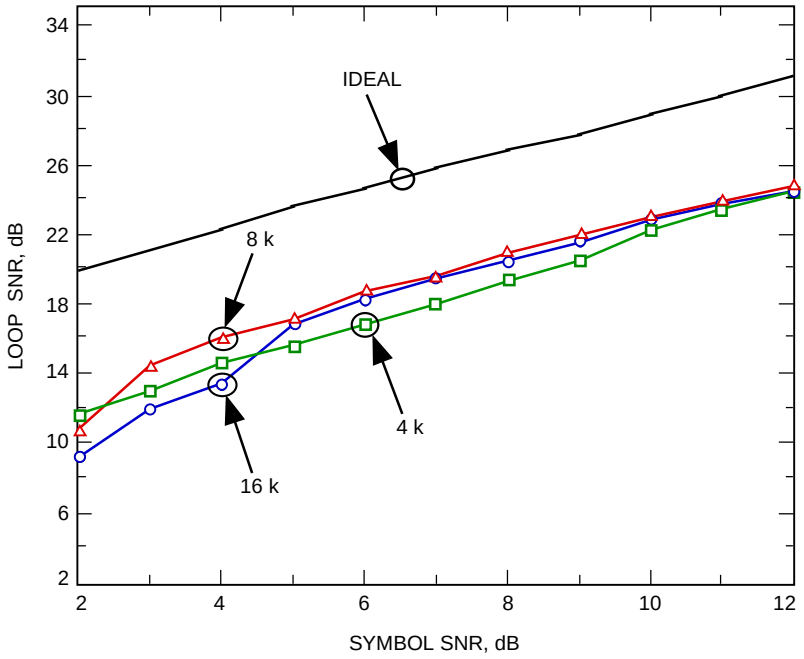

Fig. 16. Unnormalized S-curves for tracking 4-, 8-, and 16-kHz subcarriers.

Table 6. Summary of the key features for various uplink options proposed for code division multiplexing in system option no. 5.

Option	Acquisition	Carrier modulation	Bandwidth expansion	Component limiting no. of users
A	Easy	Amplitude	Small	KPA[a] or SSPA[b]
B	Hard	Phase	Large	Hard limiter
C	Easy	Quadrature amplitude	Small	KPA or SSPA
D	Hard	Phase	Small	Hard limiter

[a] Klystron power amplifier.
[b] Solid-state power amplifier.

By assuming a 0.5-dB carrier degradation limit and 30 percent of power allocated in pilot signal, one can find that, from Table 5, options A and C are able to support up to four and seven uplinks, respectively, since the peak-to-average power variation is below or around the 7-dB bound.

The key problem for options B and D is that the number of users that can be supported is greatly limited by the amount of SER performance degradation resulting from hard-limiting operation. The hard limiter destroys the orthogonality between WH code-modulated signals and, basically, introduces self-noise, which causes ambiguous mapping from each input stream to its corresponding demultiplexed stream at the receiving end. Moreover, the increased phase jitter can have a significant impact on the reliable subcarrier and symbol-timing tracking in option D since the multiplexed signal does not have symbols of rectangular pulse shape anymore.

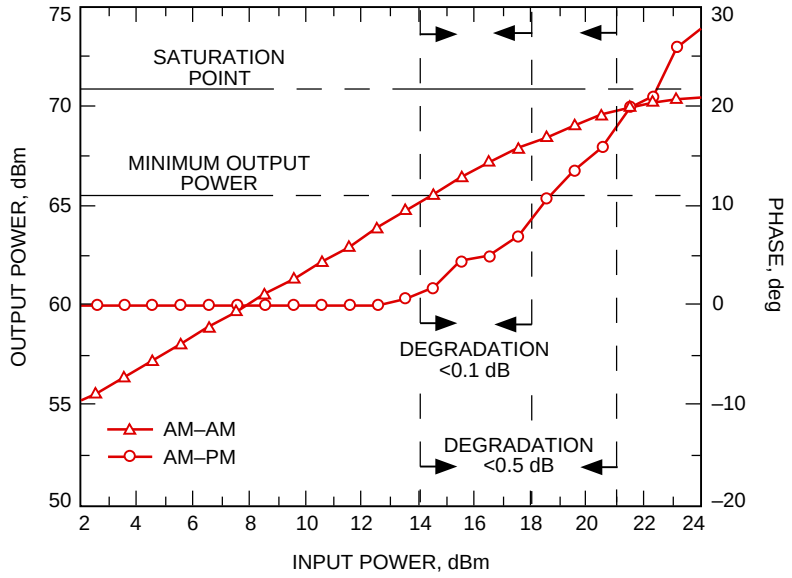

Fig. 17. Typical power amplifier characteristics for the DSN (Varian VA - 846 klystron).

Thus, among the four proposed CDM schemes presented, option D is the simplest one, requiring only minor modification to allow the different subcarrier frequencies to be used in the current S/C CDU, which makes it a very attractive short-term solution to SAML. However, the synchronization issues may prevent it from supporting more than three S/C. Option A requires more modification to the CDU by adding PN code acquisition/tracking circuits and replacing the existing subcarrier generator with a PN code generator. Option C is similar to option A, but requires a little more modification to include QAM into the CDU. Depending upon tolerances on various system aspects, option A can support a slightly higher number of users (four or five), and option C can support more users (around seven) because of the smaller power back off required. Moreover, option C has the potential to be able to support an even higher number of users by fully utilizing the capacity of QAM. (Recall that the presented option has only the pilot signal on its quadrature channel.) When under a very tight power amplifier constraint, option B can be the only choice to support a higher number of users because of its phase modulation feature. Its capacity can be expanded by concatenating several majority logic multiplexers to form a multistage unit [29]. However, an effective error control scheme should be incorporated to improve its error performance.

Based on the description of the system options, various issues and potential problems associated with this architecture are listed below:

(1) Is simultaneous command/ranging/telemetry possible?

(2) What is the PN code acquisition/tracking performance?

(3) Can codes, other than WH codes, that preserve more information after hard limiting be found?

VII. Comparison of Uplink Options

The key comparison for the CCSDSPT and CDM uplink options is the loss due to multiple users while keeping the throughput (the amount of data transmitted to all users per unit time) fixed. For instance, in CDM, the data are transmitted simultaneously to all users. In order for CCSDSPT to achieve the same throughput as CDM, the data rate for each user must be increased by a factor proportional to the

number of users. For example, for two users, the data rate for CCSDSPT must be increased by a factor of two (or 3 dB) in order to achieve the same performance (throughput) as CDM. In other words, the cost for sending the data to each S/C serially (or waiting twice as long) is 3 dB for two users. Table 7 shows the loss for CCSDSPT for users ranging from two to seven. Note that the option of CCDSDPT with SFDM has exactly the same performance as CCSDSPT under the fixed-throughput assumption, since the power has to be divided in half to support two subcarriers in the SFDM scheme. Sending the data to all the users simultaneously, as in CDM, also has a cost associated with it. For options A and C of CDM, the amount of power amplifier back off from saturation is the cost for utilizing this option. The peak-to-average power variations shown in Table 5 are added to the power loss due to the support of pilot signal and then entered in Table 7 for comparison. On the other hand, options B and D for CDM have the same performances as shown in Fig. 14 when none of the synchronization issues associated with option D are taken into consideration. These results are summarized in Table 7. Comparing CCSDSPT and CDM for the uplink for the same throughput, option C of CDM is better than other options in CDM and is comparable to the CCSDSPT option. The CCSDSPT option is the best choice in terms of its simplicity of adaptation for the current system, provided that the antenna schedule allows for sequential telecommanding for all S/C.

Table 7. Comparison of uplink SER performance in terms of loss, referenced to ideal BPSK under the same throughput assumption.

No. of users	CCSDSPT	CDM: option A[a]	CDM: options B and D[b]	CDM: option C[a]
2	3.01	6.32	5.53	3.85
3	4.77	7.56	5.53	5.35
4	6.02	8.48	8.80	6.46
5	6.99	9.22	8.80	7.35
6	7.78	9.84	8.80	8.08
7	8.45	10.37	8.80	8.71

[a] Assumes 30 percent of average power is allocated to the pilot signal.
[b] Option D is limited to support of three users.

VIII. Comparison of Downlink Options

Similar to the uplink case, the key comparison for the SFDMA, CDMA, and CFDMA with coherent TFR downlink options is the number of users that can be supported for a fixed bandwidth. The following example is used to assess the capacity of these multiple-access schemes. Let us assume that the available (two-sided) bandwidth for the downlink is 3, 10, or 30 MHz and all S/C are transmitting at a data rate of 20 kbps with a 40 dB-Hz total power-to-noise spectral level. Our goal is to find the maximum number of spacecraft that can be supported for these three schemes. An example for SFDMA has already been given in Section II.F by assuming a guard band of 500 kHz between users. Table 2 shows the loss due to finite numbers of subcarrier harmonics and the number of S/C that can be accommodated within the available bandwidths.

In order to compare CDMA with SFDMA, the total number of users that can be supported for CDMA will be determined by assuming the same total loss per user as given in Table 2. Two types of loss exist for CDMA: the filtering loss due to only a fraction of the spread spectrum (usually at chip rate) being passed through the receiver front end and, of course, the multiuser loss due to the other users occupying the same bandwidth. Table 8 shows the number of users that can be supported for a bandwidth of 3, 10,

and 30 MHz. It also shows the loss as a function of the number of nulls at which the NRZ data spectrum is filtered. It is shown that the loss for filtering at the fourth null of the spectrum is negligible (less than 0.1 dB). The number of nulls allowed in the received spectrum also indicates the spreading ratio used in the spread spectrum CDMA system. For example, the spreading ratio for 20-kbps data allowing only the first null appearing in a 30-MHz receiving bandwidth (two-sided) is 750 (15 MHz/20 kbps). Table 8 shows the spreading ratios for the other numbers of nulls. Since our goal is to compare SFDMA to CDMA for the same total loss given in Table 2, the multiuser loss for a given number of nulls is calculated such that, when added to the filtering loss, the resulting total loss corresponds to one of those losses given in Table 2. Table 8 also gives the total number of users that can be supported by CDMA, which is calculated for a given multiuser loss and a spreading ratio. Clearly, the number of users that can be supported by using CDMA is much greater than by SFDMA.

Table 8. CDMA downlink performance example for a two-sided bandwidth of 3 MHz, 10 MHz, and 30 MHz.

No. of nulls	Filtering loss, dB	Multiuser loss, dB	Total loss, dB	Spreading ratio	No. of users
			3 MHz		
1	0.43	0.48	0.91	75	27
2	0.21	0.7	0.91	37.5	14
3	0.13	0.78	0.91	25	10
4	0.1	0.81	0.91	18.75	8
			10 MHz		
1	0.43	0.48	0.91	250	89
2	0.21	0.7	0.91	125	44
2	0.21	0.25	0.45	125	15
3	0.13	0.78	0.91	83.3	33
3	0.13	0.32	0.45	83.3	13
4	0.1	0.81	0.91	62.5	26
4	0.1	0.35	0.45	62.5	11
			30 MHz		
1	0.43	0.48	0.91	750	266
2	0.21	0.09	0.3	375	17
3	0.13	0.17	0.3	250	21
4	0.1	0.2	0.3	187.5	18

CFDMA with coherent TFR is another downlink option that was discussed in system option no. 3. With a 10-MHz available bandwidth, three S/C can be supported by the Tiny DST. With a 30-MHz bandwidth, however, nine users can be supported by three 10-MHz bands, provided that the center frequency of the individual transponder exciter is mechanically tuned to support one of the three bands. The key advantage of CFDMA with coherent TFR is that the loss due to multiple access is negligible since each user is allowed a 3-MHz bandwidth. Table 9 compares the maximum number of S/C that can be supported for these three multiple-access schemes for a bandwidth of 3, 10, and 30 MHz. For the CDMA scheme in this table, one null was assumed with a 0.91-dB total loss. Consequently, the total

losses for CDMA and SFDMA are the same (0.91 dB) for the cases of 3 and 10 MHz, but for the case of a 30-MHz bandwidth, the total losses for SFDMA and CDMA are 0.3 and 0.91 dB, respectively. Clearly, CDMA is capable of supporting a much larger number of S/C than are the others.

Table 9. A comparison of the maximum number of users achievable for downlink multiple-access schemes.

Bandwidth, MHz	SFDMA	CFDMA	CDMA
3	2	1	27
10	5	3	89
30	5	9	266

IX. Conclusion and Recommendations

This article has described five system options ranging from a little to a complete modification of the current S/C transponder and ground-station DSN hardware. Table 10 shows some of the required hardware and software modifications associated with each proposed option. All of these system options are capable of supporting the SAML scenarios. Preliminary evaluation of the system performances for these options has been conducted, and the results are presented. The cost impact of the required modifications on the S/C transponder and ground-station receivers, however, has not been assessed. Moreover, the advantages, limitations, and potential problems associated with each option have been identified and summarized in Table 11. Most of the issues and problems associated with these system options have been resolved. A set of recommendations regarding which system option should be used for SAML scenarios can be derived from the findings presented throughout Sections II through VI. If one defines the criteria for selection of a proper system architecture for a short-term solution to the support of SAML as (1) a minimum hardware/software requirement, (2) an acceptable SER performance, (3) a reasonable number of user S/C (less than five S/C within the same beamwidth), (4) low-to-medium downlink data rates (40 bps to 20 kbps), (5) minimum uplink bandwidth, and (6) maximum transmission power efficiency (i.e., the power amplifier always operates at saturation), then system options no. 1, 2, and 3 appear to satisfy these requirements. In this regard, both system options no. 1 and no. 2 need only some modification in receiver software, and system option no. 3 needs a variable β factor, which will be supported by the Tiny DST. Also note that system option no. 2 provides twice the uplink throughput as compared with options no. 1 and no. 3, but at a cost of 3-dB lower symbol SNR plus some cross-modulation loss. If the criteria for a long-term solution are (1) a large number of user S/C (greater than five), (2) different uplink data rates, (3) a high downlink data rate (greater than 100 kbps), (4) maximum transmission power efficiency, and (5) minimum downlink bandwidth, then system option no. 5 seems to be the best solution. Table 12 summarizes the recommendations for the upcoming Mars and future deep-space missions that involve multiple S/C lying within the same beamwidth of the ground-station antenna. The details of operational feasibility and system design for each recommended option are still under investigation and will be addressed in subsequent articles.

Table 10. Summary of the required hardware and software modification associated with each proposed system architecture.

System option no.	Required hardware/software modifications	
	S/C transponder	Ground station
1	None	Software: –Reprogram the receiver tracking loops
2	Software: –Reprogram to track two different subcarrier frequencies	Software: –Reprogram the receiver tracking loops
3	Hardware: –Redesign of the transponder (the number of users supported depends heavily on the available frequency synthesizer technology)	None
4	Hardware: –PN code modulator	Hardware: –PN code modulator Software: –Reprogram the receiver to get Doppler/ranging data from the received PN code
5	Hardware: –None for CDM option D –PN code modulator/demodulator and WH code demodulator (except for CDM option D) –QAM demodulator for CDM option C	Hardware: –WH code and PN code modulators (except for CDM option D) and QAM modulator (only for CDM option C) –PN code demodulator Software: –Reprogram the receiver to get Doppler/ranging data from the received PN code

Table 11. Summary of the advantages, disadvantages, and limitations associated with each proposed system architecture.

System option no.	Advantage	Disadvantage
1	–Conforms with CCSDS standards for both uplink and downlink –No uplink bandwidth expansion –Very good uplink and acceptable downlink SER performances	–Cannot acquire additional S/C after the initial locking on S/C in view –Requires large downlink bandwidth –Potential loss due to interchannel interference (maximum number of supported S/C is less than five
2	–Same as option no. 1 –Double the uplink throughput as compared with option no. 1	–Same as option no. 1 –Uplink SER is worse than that of option no. 1 (3 dB plus an additional 0.2- to 0.5-dB degradation due to cross-modulation
3	–Same as option no. 1 –Better downlink SER performance as compared with options nos. 1 and 2	–S/C hardware modification –Tiny DST required
4	–Same as option no. 1 for uplink –Can support high-rate downlinks –Can support a larger number of user S/C (much more than five) –Can derive ranging information from the PN code	–Requires hardware/software modification –Potential downlink acquisition problem due to low SNR and two-way Doppler/Doppler rate –Downlink does not conform with the CCSDS standards
5	–Same as option no. 4 for downlink –Can support different uplink data rates –Can support high-rate uplink –Can support a larger number of user S/C (much more than five)	–Requires complete modification of both S/C and ground station hardware/software –Does not conform with the CCSDS standards

Table 12. Recommendations for short- and long-term solutions for SAML scenarios.

Solution	Recommended option	Remarks
Short-term	Option no. 1: CCSDSPT for the uplink and SFDMA for the downlink	–No hardware modification –Conforms with CCSDS recommendations –Acceptable downlink performance –Maximum number of S/C it can support is less than five –Cannot support (1) variable rates on the uplink and (2) a high data rate on the downlink
	Option no. 2: CCSDSPT/SFDM for the uplink and SFDMA for the downlink	–Same as option no. 1 except that the uplink throughput is doubled at the expense of a 3-dB lower symbol SNR plus a 0.2- to 0.5-dB cross-modulation loss
	Option no. 3: CCSDSPT for the uplink and coherent ATFR for the downlink	–Same as option no. 1 with better downlink SER performance –Tiny DST is needed to support ATFR
Long-term	Option no. 5: CDM with Walsh–Hadamard function for the uplink and CDMA for the downlink	–Complete redesign of both S/C and ground-station hardware/software is required –Can support more than five S/C with variable rates on the uplink and a high data rate on the downlink

Acknowledgments

The authors would like to thank the members of the Single Aperture Multi-Link Team at JPL for many useful discussions, Dave Bell for providing the Doppler profiles, Fernando Peralta for the Doppler calculation, Bruce Conroy and Daniel Hoppe for providing the power amplifier characteristics, and Ann Devereaux for her valuable comments and suggestions. Finally, the authors would like to thank Warren L. Martin for his continuous support of this study.

References

[1] T. M. Nguyen, S. M. Hinedi, W. L. Martin, and H. Tsou, "Communication System Architectures for Missions to Mars-A Preliminary Investigation," presented at IEEE International Conference on Communications (ICC'95), Seattle, Washington, June 18–22, 1995.

[2] International Consultative Committee for Space Data Systems, CCSDS, *Recommendations for Space Data System Standards, Telecommand, Part I, Channel Service, Architectural Specification*, CCSDS 201.0-B-1, Blue Book, January 1987.

[3] D. A. Bathker, D. W. Brown, and S. M. Petty, *Single- and Dual-Carrier Microwave Noise Abatement in the Deep Space Network*, JPL Technical Memorandum 33-733, Jet Propulsion Laboratory, Pasadena, California, August 1, 1975.

[4] B. L. Conroy and D. J. Hoppe, "Noise Bursts and Intermodulation Products Caused by Multiple Carriers at X-Band," *The Telecommunications and Data Acquisition Progress Report 42-127, July–September 1996*, Jet Propulsion Laboratory, Pasadena, California, pp. 1–8, November 15, 1996.
http://tda.jpl.nasa.gov/tda/progress_report/42-127/127E.pdf

[5] International Consultative Committee for Space Data Systems, CCSDS, *Recommendations for Space Data System Standards, Radio Frequency and Modulation Systems, Part I, Earth Stations and Spacecraft*, CCSDS 401.0-B, Blue Book, 1989.

[6] International Consultative Committee for Space Data Systems, CCSDS, *Recommendations for Space Data System Standards, Telecommand, Part II, Data Routing Service, Architectural Specification*, CCSDS 202.0-B-2, Blue Book, November 1992.

[7] F. J. MacWilliams and N. J. A. Sloane, *The Theory of Error Correcting Codes*, The Netherlands: Elsevier Science Publishers B. V., 1977.

[8] S. Lin and D. J. Costello, *Error Control Coding: Fundamentals and Applications*, Englewood Cliffs, New Jersey: Prentice-Hall, 1983.

[9] T. M. Nguyen, "Technique to Select the Optimum Modulation Indices for Suppression of Undesired Signals for Simultaneous Range and Data Operations," *IEEE Transactions on Electromagnetic Compatibility*, vol. 32, no. 1, pp. 9–17, February 1990.

[10] J. K. Holmes, Coherent Spread Spectrum Systems, New York: John Wiley and Sons, 1982.

[11] E. Youssefzadeh, *Satellite and Ground Station Intermodulation in Single Channel Per Carrier Systems*, Communication Satellite Planning Center Technical Report no. 7, Radio Science Laboratory, Standford Electronic Laboratory, June 1976.

[12] M. K. Simon, J. K. Omura, R. A. Scholtz, and B. K. Levitt, *Spread Spectrum Communications Handbook*, New York: McGraw-Hill, 1994.

[13] L. Lam and S. Million, "Performance of PCM/PM Receivers With Non-Ideal Data," presented at the CCSDS RF and Modulation Subpanel 1E Meeting, Pasadena, California, May 1996.

[14] J. A. Koukous, "Selection of Ka-Band Transponder Turn-Around Frequency Ratios," *Report of the Proceedings of the RF & Modulation, Subpanel 1E Meeting at the GSOC*, Consultative Committee for Space Data Systems, Oberpfaffenhofen, Germany, September 20–24, 1993, CCSDS B20.0-Y-1, Yellow Book, February 1994.

[15] I. Galton and G. Zimmerman, "Combined RF Phase Extraction and Digitization," presented at the 1993 International Symposium on Circuits and Systems (ISCAS'93).

[16] R. L. Peterson, R. E. Ziemer, and D. E. Booth, *Introduction to Spread Spectrum Communications*, Englewood Cliffs, New Jersey: Prentice-Hall, 1995.

[17] *Mobile Station-Base Station Compatibility Standard for Dual-Mode Wideband Spread Spectrum Cellular System*, TIA/EIA/IS-95, Telecommunication Industry Association, July 1993.

[18] A. J. Viterbi, *CDMA Principles of Spread Spectrum Communication*, Reading, Massachusetts: Addison-Wesley Publishing Company, 1995.

[19] M. Otter, "Characteristics of Various PN Codes Families for Typical Spread Spectrum Applications," *Report of the Proceedings of the RF and Modulation Subpanel 1E Meeting at the AMES Research Center*, Consultative Committee for Space Data Systems, Moffett Field, California, April 11-20, 1989, CCSDS 421.0-G1, Green Book, September 19, 1989.

[20] D. V. Sarwate and M. B. Pursley, "Cross-Correlation Properties of Pseudorandom and Related Sequences," *Proceedings of the IEEE*, vol. 68, no. 5, pp. 593–619, May 1980.

[21] K. G. Beauchamp, *Applications of Walsh and Related Functions, With an Introduction to Sequency Theory*, London: Academic Press, 1984.

[22] J. H. van Lint and R. M. Wilson, *A Course in Combinatorics*, Cambridge, England: Cambridge University Press, 1992.

[23] T. M. Nguyen, *Phase Ambiguity Resolution for QPSK Modulation, Part II: A Method to Resolve the Phase-Ambiguity for Offset QPSK Modulation Systems*, JPL Publication 89-4, Part II, Jet Propulsion Laboratory, Pasadena, California, May 15, 1989.

[24] L. R. Welch, "Lower Bounds on the Maximum Cross Correlation of Signals," *IEEE Transactions on Communications*, vol. COM-18, pp. 606–612, 1974.

[25] S. Golomb, *Shift Register Sequences*, San Francisco: Holden-Day, 1967.

[26] S. Golomb et al., *Digital Communications With Space Applications*, Englewood Cliffs, New Jersey: Prentice-Hall, 1964.

[27] R. Gold, "Maximal Recursive Sequence With Multi-Valued Cross Correlation," *IEEE Transactions on Information Theory*, vol. IT-14, pp. 154–156, 1968.

[28] T. Kasami and L. Lin, "Coding for Multiple Access Channels," *IEEE Transactions on Information Theory*, vol. IT-22, pp. 123–132, 1976.

[29] J. A. Gordon and R. Barrett, "Group Multiplexing by Concatenation of Non-Linear Code Division Systems," *Proceedings of Applications of Walsh Functions Symposium*, AD 744650, Naval Research Laboratory, Washington, DC, pp. 73–81, 1972.

[30] J. A. Gordon and R. Barrett, "Correlation-Recovered Adaptive Majority Multiplexing," *Proceedings of IEE*, vol. 118, no. 3/4, pp. 417–422, March/April 1971.

Appendix A
Sample Design Control Tables

In this appendix, the link design control tables for some sample uplinks and downlinks in X-band are provided in Figs. A-1 through A-4 for the proposed mission to Mars. The key assumptions used for the Mars orbiters were as follows:

(1) A 1.5-m high-gain antenna (HGA) with a gain of 38.6 dBi.

(2) Uplink telecommand data rates of 500 bps and 2 kbps.

(3) Downlink telemetry data rates of 10 kbps and 20 kbps.

(4) A Viterbi encoded (7,1/2) telemetry channel.

(5) A maximum range of 2.67 AU.

For the Mars landers, the assumptions were identical to the Mars orbiters except that (1) the low-gain antenna (LGA) had a 9.2-dBi gain and (2) the downlink data rates were 10 bps to 40 bps. It was assumed for the analysis that the standard PCM/PSK/PM modulation with sine-wave subcarrier for the uplink and square-wave for the downlink was used. The ground station was assumed to be a 20-kW DSN 34-m HEF antenna. Under these conditions, the received carrier power from the uplink calculations was -112.4 dBm for the Mars orbiters and -140 dBm for the Mars landers, which was an important parameter for the onboard phase-locked loop performance. Moreover, the link performance margin is the bottom line of a link design; a positive link margin is necessary to ensure successful operation and provide sufficient buffer against adverse situations.

HGA UPLINK
DSN 20 kW/34m HEF station/blind pointing/0.012 deg peak error
Canberra/25 deg elevation/8 10-5, Rev. C weather model
X-band HGA/3.14 mrad pointing error/No hot body noise
1.5m diam
X-band/SDST/best estimates/8.75 Hz BLo
Command channel/uncoded, PB=1E–5 *500.00 bps*
Sine wave subcarrier/new model

									Date	
									DOM	
									DOY	
								3.994E+08	Range, km	
								2.67	Range, AU	
								0.37	OWLT, hrs	
								25	Elev. Angle	
	Link Parameter	Unit	Design Value	Fav Tol	Adv Tol	Mean Value	Var	Shape		
	TRANSMITTER PARAMETERS									
1	Total Xmitter Pwr	dBm	73.01	0.20	–0.20	73.01	0.0067	T	20	Xmtr Pwr, kW
2	Xmitter Waveguide Loss	dB	–0.25	0.05	–0.05	–0.25	0.0004	T		
3	DSN Antenna Gain	dBi	67.12	0.20	–0.20	67.12	0.0134	U	45	DSS antenna
4	Ant Pointing Gain	dB	–0.10	0.10	–0.10	–0.10	0.0017	T		
5	EIRP (1+2+3+4)	dBm				139.78	0.0221	U		
									X	RF band
	PATH PARAMETERS									
6	Space Loss	dB	–281.59			–281.59		D	7175.03	Freq, MHz
7	Atmospheric Attn	dB	–0.28			–0.28		D	99	Weather %
	RECEIVER PARAMETERS									
8	Polarization Loss	dB	–0.09	0.08	–0.06	–0.08	0.0017	U		
9	Ant Pointing Loss	dB	0.00	0.00	–1.00	–0.33	0.0556	T		
10	S/C Antenna Gain	dBi	36.61	0.40	–0.60	36.54	0.0432	T	1.5m diam	
11	Lumped Ckt/Ant Loss	dB	–2.20	0.32	–0.41	–2.25	0.0445	U	HGA	S/C Antenna
	TOTAL POWER SUMMARY									
12	Total Rcvd Pwr (Pt) (5+6+7+8+9+10+11)	dBm				–108.22	0.1662	G		
13	Noise Spec Dens	dBm/Hz	–174.19	–0.27	0.67	–174.06	0.0394	T		
	System Noise Temp	K	275.92	–16.83	46.10					
	Rcvr Noise Temp	K	159.16	–10.22	43.33					
	Rcvr Noise Figure	dB	1.90	–0.10	0.40					
	Loss Noise Contr.	K	115.26	–13.36	15.74					
	Hot Body Contrib.	K	1.51	–0.14	0.12					
14	Rcvd Pt/No	dB-Hz				65.84	0.2056	G	(12–13)	
	CARRIER PERFORMANCE									
15	Cmd Carrier Supp	dB	–4.15	0.20	–0.20	–4.15	0.0067	T	TRUE	CMD.MOD
16	Rng Carrier Supp	dB	0.00	0.00	0.00	0.00	0.0000	T	FALSE	RNG.MOD
17	Rcvd Carr Power (Pc)	dBm				–112.37	0.1729	T	(12+15+16)	
18	Carr Noise BW, 2BLo	dB-Hz	12.43	1.00	–0.71	12.58	0.2443	U	17.5	Hz
19	Required Carrier Margin	dB	12.00			12.00		D		
20	Excess Carrier Margin	dB				37.11	0.4565	U	(17–13–18–19)	
	CHANNEL PERFORMANCE									
21	Cmd Modulation Loss	dB	–2.64	–0.10	–0.10	–2.64	0.0017	T	1.3	cmd MI, rad
22	Rng Data Supp	dB	0.00	0.00	0.00	0.00	0.0000	T	44.9	rng MI, deg
23	Data Pwr to Rcvr (Pd)	dBm				–110.85	0.1679	T	(12+21+22)	
24	Data Rate	dB	26.99	0.00	0.00	26.99	0.0000	D	500	data rate
25	Eb/No	dB				36.22	0.2073	T	(14+21+22–24)	
26	System Loss	dB	–0.80	0.28	–0.28	–0.80	0.0131	T	(includes radio loss)	
27	Threshold Eb/No	dB	9.60			9.60		D	BER = 1E–5, uncoded	
28	Performance Margin	dB				25.82	0.2073	T	(25+26–27)	
29	Sigma	dB				0.46				
30	Margin - 3 Sigma	dB				24.45				

Fig. A-1. SAML uplink design control table for Mars orbiter.

LGA Uplink
DSN 20 kW/34m HEF station/blind pointing/0.012 deg peak error
Canberra/25 deg elevation/8 10-5, Rev. C weather model
X-band LGA/No hot body noise
Antenna pointing error *0.0 deg*
X-band/SDST/best estimates/8.75 Hz BLo
Command channel/uncoded, PB=1E–5 *500.00 bps*
Sine wave subcarrier/new model

									Date	
									DOM	
									DOY	
								3.994E+08	Range, km	
								2.67	Range, AU	
								0.37	OWLT, hrs	
								25	Elev. Angle	
	Link Parameter	Unit	Design Value	Fav Tol	Adv Tol	Mean Value	Var	Shape		
	TRANSMITTER PARAMETERS									
1	Total Xmitter Pwr	dBm	73.01	0.20	–0.20	73.01	0.0067	T	20	Xmtr Pwr, kW
2	Xmitter Waveguide Loss	dB	–0.25	0.05	–0.05	–0.25	0.0004	T		
3	DSN Antenna Gain	dBi	67.12	0.20	–0.20	67.12	0.0134	U	45	DSS antenna
4	Ant Pointing Gain	dB	–0.10	0.10	–0.10	–0.10	0.0017	T		
5	EIRP (1+2+3+4)	dBm				139.78	0.0221	U		
									X	RF band
	PATH PARAMETERS									
6	Space Loss	dB	–281.59			–281.59		D	7175.03	Freq, MHz
7	Atmospheric Attn	dB	–0.28			–0.28		D	99	Weather %
	RECEIVER PARAMETERS									
8	Polarization Loss	dB	–0.10	0.09	–0.08	–0.10	0.0023	U		
9	Ant Pointing Loss	dB	0.00	0.00	0.00	0.00	0.0000	T		
10	S/C Antenna Gain	dBi	9.20	0.00	0.00	9.20	0.0000	T		Pointing angle
11	Lumped Ckt/Ant Loss	dB	–2.85	0.50	–0.58	–2.89	0.0974	U	LGA	S/C Antenna
	TOTAL POWER SUMMARY									
12	Total Rcvd Pwr (Pt)	dBm				–135.88	0.1219	G		
	(5+6+7+8+9+10+11)									
13	Noise Spec Dens	dBm/Hz	–173.83	–0.32	0.64	–173.72	0.0391	T		
	System Noise Temp	K	300.00	–21.01	47.24					
	Rcvr Noise Temp	K	159.16	–10.22	43.33					
	Rcvr Noise Figure	dB	1.90	–0.10	0.40					
	Loss Noise Contr.	K	139.55	–18.36	18.81					
	Hot Body Contrib.	K	1.30	–0.16	0.16					
14	Rcvd Pt/No	dB-Hz				37.84	0.1610	G	(12–13)	
	CARRIER PERFORMANCE									
15	Cmd Carrier Supp	dB	–4.15	0.20	–0.20	–4.15	0.0067	T	TRUE	CMD.MOD
16	Rng Carrier Supp	dB	0.00	0.00	0.00	0.00	0.0000	T	FALSE	RNG.MOD
17	Rcvd Carr Power (Pc)	dBm				–140.03	0.1286	T	(12+15+16)	
18	Carr Noise BW, 2BLo	dB-Hz	12.43	1.00	–0.71	12.58	0.2443	U	17.5	Hz
19	Required Carrier Margin	dB	12.00			12.00		D		
20	Excess Carrier Margin	dB				9.11	0.4119	U	(17–13–18–19)	
	CHANNEL PERFORMANCE									
21	Cmd Modulation Loss	dB	–2.64	0.10	–0.10	–2.64	0.0017	T	1.3	cmd MI, rad
22	Rng Data Supp	dB	0.00	0.00	0.00	0.00	0.0000	T	44.9	rng MI, deg
23	Data Pwr to Rcvr (Pd)	dBm				–138.52	0.1236	T	(12+21+22)	
24	Data Rate	dB	26.99	0.00	0.00	26.99	0.0000	D	500	data rate
25	Eb/No	dB				8.22	0.1627	T	(14+21+22–24)	
26	System Loss	dB	–0.80	0.28	–0.28	–0.80	0.0131	T	(includes radio loss)	
27	Threshold Eb/No	dB	9.60			9.60		D	BER = 1E–5, uncoded	
28	Performance Margin	dB				–2.18	0.1627	T	(25+26–27)	
29	Sigma	dB				0.40				
30	Margin - 3 Sigma	dB				–3.39				

Fig. A-2. SAML uplink design control table for Mars lander.

X-band/20 W TWTA/BOL Value/For Cruise										Date
HGA Gain: 38.63 dBi										DOM
										DOY
DSN 34 m station/X-band/diplexed/maser									399432000	Range, km
Canberra /25.0 deg elevation/810-5, Rev. C weather model									2.67	Range, AU
Hot body noise: none					*Loop Bandwidth:*		*0.5 Hz*		0.37	OWLT, hrs
DSN Block V receiver/residual carrier mode										
Tlm channel/Viterbi (7, 1/2), PB=1.E–5					*20000 bps*				25	Elev. Angle
	Link Parameter	Unit	Design Value	Fav Tol	Adv Tol	Mean Value	Var	Shape		
	TRANSMITTER PARAMETERS									
1	S/C RF Power Output	dBm	44.31	0.50	–0.50	44.31	0.0417	T	27	Xmtr Pwr, W
2	Xmitter Circuit Loss	dB	–1.10	0.30	–0.50	–1.20	0.0535	U		
3	Antenna Circuit Loss	dB	–0.20	0.10	–0.10	–0.20	0.0033	U		
4	Antenna Gain	dBi	38.66	0.60	–0.60	38.66	0.0601	T		
5	Ant Pointing Loss	dB	0.00	0.00	–1.00	–0.33	0.0556	T	HGA	S/C Antenna
6	Spacecraft EIRP	dBm				81.24			min req'd EIRP	79.04
	PATH PARAMETERS									
7	Space Loss	dB	–282.99	0.00	0.00	–282.99	0.0000	D	X	RF band
8	Atmospheric Attn	dB	–0.14	0.00	0.00	–0.14	0.0000	D	8429.94	Freq, MHz
	RECEIVER PARAMETERS									
9	DSN Antenna Gain	dBi	68.08	0.20	–0.20	68.08	0.0134	U	90	Weather %
10	Ant Pointing Loss	dB	–0.10	0.00	0.00	–0.10	0.0000	U	45	DSS antenna
11	Polarization Loss	dB	–0.04	0.00	0.00	–0.04	0.0000	U		
	TOTAL POWER SUMMARY									
12	Total Rcvd Pwr (Pt) (6+7+8+9+10+11)	dBm				–133.96	0.2276	G	req'd rcv'd pwr	–136.16
13	Noise Spec Dens	dBm/Hz	–183.08	–0.25	0.24	–183.09	0.0062	G		
	System Noise Temp	K	35.65	–2.00	2.00			G	2	Way
	Zenith NT	K	26.60	–2.00	2.00	26.60	0.6675	T		
	Elevation	K	0.26	0.00	0.00	0.26	0.0000	G		
	Clouds	K	8.79	0.00	0.00	8.79	0.0000	G		
	Hot Body Noise	K	0.00	0.00	0.00	0.00	0.0000	G		
14	Available Pt/No	dB-Hz				49.13	0.2338	G		
	CARRIER PERFORMANCE									
15	TLM Carrier Supp	dB	–15.21	1.27	–1.50	–15.28	0.3220	T	TRUE	TLM.MOD
16	Rng Carrier Supp	dB	0.00	0.00	0.00	0.00	0.0000	T	FALSE	RNG.MOD
17	DOR Carrier Supp	dB	0.00	0.00	0.00	0.00	0.0000	T	FALSE	DOR.MOD
18	Rcvd Carr Pwr (Pc)	dBm				–149.24	0.5496	T		
19	Carrier Loop Bandwidth, Bl	dB-Hz	6.99	0.00	0.00	6.99	0.0000	T	5	RF.BW.SELECT
20	Carrier Loop SNR	dB				26.86	0.5559	U		
21	Required Carrier Loop SNR	dB				10.00	0.0000	D		
22	Carrier Loop SNR Margin	dB				16.86	0.5559	U		
	TELEMETRY PERFORMANCE									
23	Tlm Data Supp	dB	–0.13	0.04	–0.05	–0.04	0.0003	T	80.0	tlm, MI deg
24	Rng Data Supp	dB	0.00	0.00	0.00	0.00	0.0000	T	0.00	rng MI, deg
25	DOR Data Supp	dB	0.00	0.00	0.00	0.00	0.0000	T	0.00	dor 1 MI, rad
26	Data Rate	dB	43.01	0.00	0.00	43.01	0.0000	D	0.00	dor 2 MI, rad
27	Eb/No to Receiver	dB				5.98	0.2341	T	20000	data rate
28	System Losses	dB	0.00	0.00	0.00	0.00	0.0000	T		
29	Eb/No Output	dB				5.98	0.2341	T		
30	Threshold Eb/No	dB				2.81	0.0000	D		
31	Performance Margin	dB				3.17	0.2341	T		
32	Sigma	dB				0.48				
33	Margin - 2 Sigma	dB				2.20				

Fig. A-3. SAML downlink design control table for Mars orbiter.

X-band/20 W TWTA/BOL Value/For Cruise
LGA Gain: 9.2 dBi

DSN 34 m station/X-band/diplexed/maser
Canberra /25.0 deg elevation/810-5, Rev. C weather model
Hot body noise: none *Loop Bandwidth:* *0.5 Hz*
DSN Block V receiver/residual carrier mode
Tlm channel/Viterbi (7, 1/2), PB=1.E–5 *40 bps*

									Date	
									DOM	
									DOY	
								399432000	Range, km	
								2.67	Range, AU	
								0.37	OWLT, hrs	
								25	Elev. Angle	
	Link Parameter	Unit	Design Value	Fav Tol	Adv Tol	Mean Value	Var	Shape		
	TRANSMITTER PARAMETERS									
1	S/C RF Power Output	dBm	44.31	0.50	–0.50	44.31	0.0417	T	27	Xmtr Pwr, W
2	Xmitter Circuit Loss	dB	–1.30	0.30	–0.50	–1.40	0.0535	U		
3	Antenna Circuit Loss	dB	–0.65	0.30	–0.30	–0.65	0.0301	U		
4	Antenna Gain	dBi	9.20	0.00	0.00	9.20	0.0000	T	0.0	Pointing Angle
5	Ant Pointing Loss	dB	0.00	0.00	0.00	0.00	0.0000	T	LGA	S/C Antenna
6	Spacecraft EIRP	dBm				51.46			min req'd EIRP	52.63
	PATH PARAMETERS									
7	Space Loss	dB	–282.99	0.00	0.00	–282.99	0.0000	D	X	RF band
8	Atmospheric Attn	dB	–0.14	0.00	0.00	–0.14	0.0000	D	8429.94	Freq, MHz
	RECEIVER PARAMETERS									
9	DSN Antenna Gain	dBi	68.28	0.20	–0.20	68.28	0.0134	U	90	Weather %
10	Ant Pointing Loss	dB	–0.10	0.00	0.00	–0.10	0.0000	U	45	DSS antenna
11	Polarization Loss	dB	–0.13	0.12	–0.10	–0.12	0.0043	U		
	TOTAL POWER SUMMARY									
12	Total Rcvd Pwr (Pt) (6+7+8+9+10+11)	dBm				–163.61	0.1429	G	req'd rcv'd pwr	–162.45
13	Noise Spec Dens	dBm/Hz	–184.35	–0.34	0.31	–184.36	0.0112	G		
	System Noise Temp	K	26.60	–2.00	2.00			G	1	Way
	Zenith NT	K	17.55	–2.00	2.00	17.55	0.6675	T		
	Elevation	K	0.26	0.00	0.00	0.26	0.0000	G		
	Clouds	K	8.79	0.00	0.00	8.79	0.0000	G		
	Hot Body Noise	K	0.00	0.00	0.00	0.00	0.0000	G		
14	Available Pt/No	dB-Hz				20.75	0.1541	G		
	CARRIER PERFORMANCE									
15	TLM Carrier Supp	dB	–3.87	0.18	–0.19	–3.88	0.0056	T	TRUE	TLM.MOD
16	Rng Carrier Supp	dB	0.00	0.00	0.00	0.00	0.0000	T	FALSE	RNG.MOD
17	DOR Carrier Supp	dB	0.00	0.00	0.00	0.00	0.0000	T	FALSE	DOR.MOD
18	Rcvd Carr Pwr (Pc)	dBm				–167.49	0.1485	T		
19	Carrier Loop Bandwidth, Bl	dB-Hz	6.99	0.00	0.00	6.99	0.0000	T	5	RF.BW.SELECT
20	Carrier Loop SNR	dB				9.88	0.1597	U		
21	Required Carrier Loop SNR	dB				10.00	0.0000	D		
22	Carrier Loop SNR Margin	dB				–0.12	0.1597	U		
	TELEMETRY PERFORMANCE									
23	Tlm Data Supp	dB	–2.29	0.12	–0.13	–2.29	0.0027	T	50.2	tlm, MI deg
24	Rng Data Supp	dB	0.00	0.00	0.00	0.00	0.0000	T	0.00	rng MI, deg
25	DOR Data Supp	dB	0.00	0.00	0.00	0.00	0.0000	T	0.00	dor 1 MI, rad
26	Data Rate	dB	16.02	0.00	0.00	16.02	0.0000	D	0.00	dor 2 MI, rad
27	Eb/No to Receiver	dB				2.44	0.1568	T	40	data rate
28	System Losses	dB	0.00	0.00	0.00	0.00	0.0000	T		
29	Eb/No Output	dB				2.44	0.1568	T		
30	Threshold Eb/No	dB				2.81	0.0000	D		
31	Performance Margin	dB				–0.37	0.1568	T		
32	Sigma	dB				0.40				
33	Margin - 2 Sigma	dB				–1.16				

Fig. A-4. SAML downlink design control table for Mars lander.

Appendix B
Sample X-Band Doppler Profiles

In this appendix, the X-band (8450-MHz) one-way and two-way Doppler profiles for two 300-km-altitude Mars orbiting S/C and an equatorial Mars lander are provided as Doppler shift (in kHz) versus time (in minutes) in Fig. B-1. The basic assumptions of the calculated profiles are as given in Table B-1.

In the Fig. B-1 plots, the Doppler figure is set to zero when the planet obscures the view of the transmitter. While the lander can be seen at most over 180 deg of Mars' revolution, the orbiters can be seen for 226.6 deg of their orbits. It is shown that all three users (two orbiters and one lander) can be seen simultaneously for about 20 percent of a day.

Table B-1. Basic assumptions of the X-band Doppler profiles.

Parameter	Value
Mars radius	3.39×10^6 m
Mars revolution time	88,560 s
Mars tangential velocity	241 m/s
Orbit radius	3.69×10^6 m
Orbit time	6806 s
Orbiter tangential velocity	3410 m/s
Orbiters' separation	120 deg

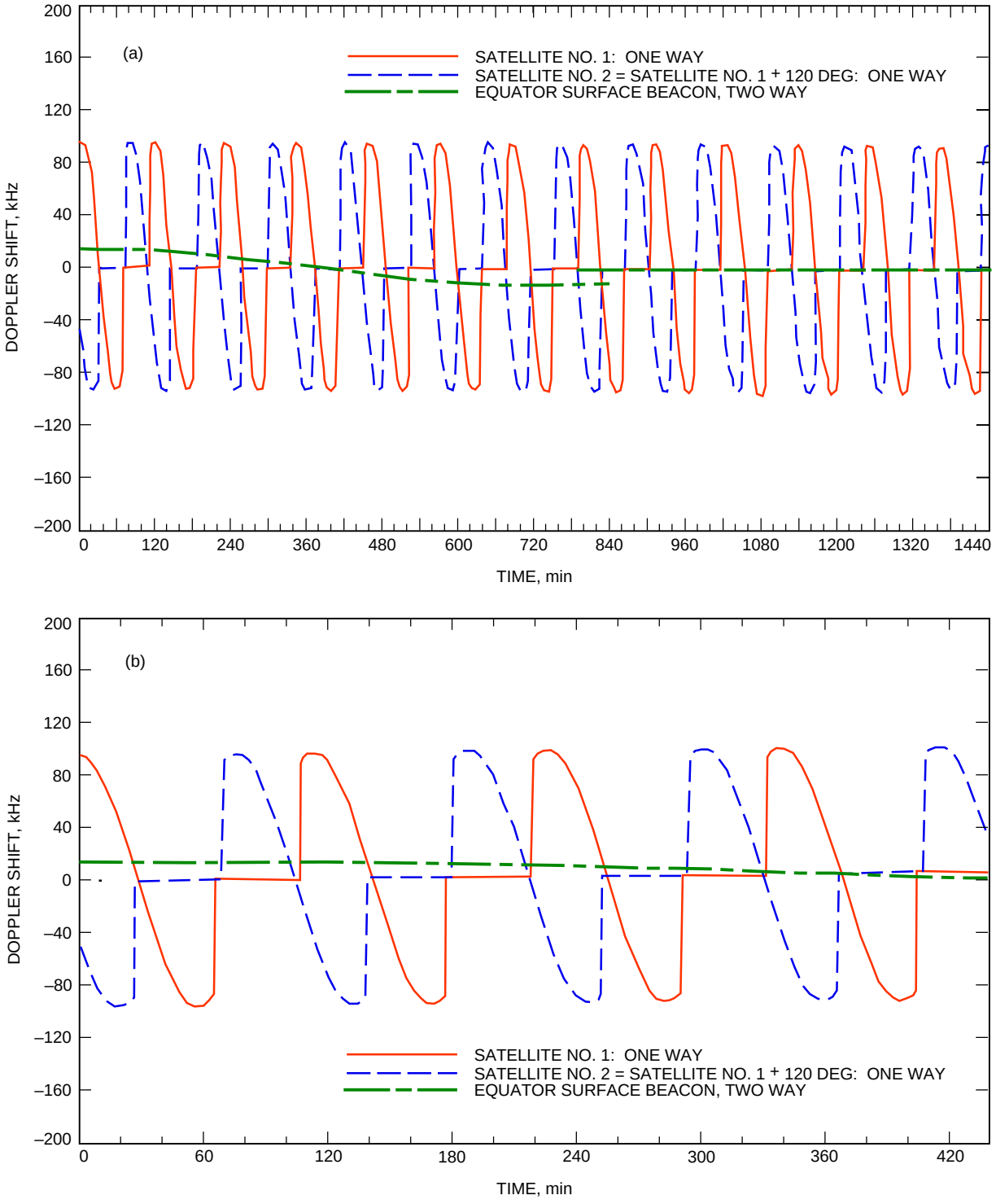

Fig. B-1. As viewed from Earth for two 300-km altitude Mars orbiters and a lander beacon at the Mars equator, with an 8450-MHz transmission frequency: (a) the Doppler profile and (b)an enlargement of the profile.

Appendix C

Effect of Unsuppressed-Carrier Components in the Costas Loop

One method for generating a suppressed-carrier binary signal is to phase modulate a carrier with a binary modulation using a 90-deg modulation angle. The case of interest here is when the binary modulation consists of a BPSK-modulated square-wave subcarrier. As such, the transmitter generates the signal

$$S(t) = \sqrt{2P}\sin(2\pi f_c t + \theta_m d(t) Sq(2\pi f_{sc} t) + \theta_c) \tag{C-1}$$

where P denotes the signal power, f_c is the carrier frequency, f_{sc} is the subcarrier frequency, $d(t)$ is the binary data signal at rate $1/T_b$ with rectangular pulse, θ_c is the carrier phase, and θ_m is the modulation angle, which, as stated above, is ideally equal to 90 deg. When θ_m is less than 90 deg due to a nonideal phase modulator, then a discrete carrier component will exist in the power spectrum. This can be seen immediately by applying simple trigonometry to Eq. (C-1), namely,

$$S(t) = \sqrt{2P_c}\sin(2\pi f_c t + \theta_c) + \sqrt{2P_d} d(t) Sq(2\pi f_{sc} t)\cos(2\pi f_c t + \theta_c) \tag{C-2}$$

where

$$\left.\begin{aligned} P_c &\triangleq P\cos^2\theta m \\ P_d &\triangleq P\sin^2\theta m \end{aligned}\right\} \tag{C-3}$$

The first term in Eq. (C-2) is a discrete carrier component, while the second term is the desired suppressed-carrier, data-modulated square wave.

Consider an I–Q Costas loop with embedded subcarrier demodulation with input $r(t) = s(t) + n(t)$, where $n(t)$ is additive Gaussian noise with single-sided power spectral density N_0 W/Hz. Assuming perfect subcarrier demodulation, the I and Q integrate-and-dump (I&D) outputs are given by

$$\begin{aligned} y_c(t) &= \int_0^{T_b} r(t)\sqrt{2}\cos(2\pi f_c t + \hat{\theta}_c) Sq(2\pi f_{sc} t) dt \\ &= \sqrt{P_c}\sin\phi_c \int_0^{T_b} Sq(2\pi f_{sc} t) dt + \sqrt{P_d}\cos\phi_c \int_0^{T_b} Sq^2(2\pi f_{sc} t) dt + N_c \\ &= \sqrt{P_d} T_b \cos\phi_c + N_c \end{aligned} \tag{C-4a}$$

and

$$y_s(t) = \int_0^{T_b} r(t)(-\sqrt{2}\sin(2\pi f_c t + \hat{\theta}_c))Sq(2\pi f_{sc}t)dt$$

$$= -\sqrt{P_c}\cos\phi_c \int_0^{T_b} Sq(2\pi f_{sc}t)dt + \sqrt{P_d}\sin\phi_c \int_0^{T_b} Sq^2(2\pi f_{sc}t)dt + N_s$$

$$= \sqrt{P_d}T_b \sin\phi_c + N_s \tag{C-4b}$$

where f_c is the estimated carrier phase error, N_c and N_s are independent zero-mean Gaussian random variables with variance $N_0T_b/2$, and we have assumed either an integer number of subcarrier cycles per bit or, instead, a large ratio of subcarrier frequency-to-bit rate. Aside from the reduction of the power in the data signal from the total power P to P_d, the I&D outputs in Eq. (C-4) are identical to what would be obtained in a conventional Costas loop operating on a fully suppressed data-modulated carrier. Thus, we conclude that the presence of an unsuppressed-carrier component caused by an imperfect phase modulator that produces a modulation angle of less than 90 deg does not degrade the performance other than to reduce the effective power in the data component by $(\cos\theta_m)^2$.

Appendix D

Families of Codes for Code Division Multiple Access

This appendix is intended to summarize briefly the key results of three families of codes that can be used for deep-space code division multiple-access (CDMA) applications. In CDMA, simultaneous communication of multiple users in the same frequency band is possible, where each user is assigned a unique pseudonoise (PN) code that has good auto-correlation and cross-correlation properties. Mathematically, the periodic auto- and cross-correlation can be described as

$$P_{aa}(\tau) = \sum_{n=1}^{N} a_{n+\tau}a_n \tag{D-1}$$

$$P_{ab}(\tau) = \sum_{n=1}^{N} a_{n+\tau}b_n \tag{D-2}$$

respectively, where the the sequences a_n and b_n are periodic with period N. The auto-correlation is the correlation between a sequence and a time-shifted version of itself and is important for code acquisition and tracking. The cross-correlation, on the other hand, is the correlation between two different code sequences and is important for interference suppression. The maximum auto- and cross-correlation magnitudes are defined as

$$P_A = \max_{0<\tau<N} |P_{aa}(\tau)| \tag{D-3}$$

$$P_C = \max_{0\leq\tau<N} |P_{ab}(\tau)| \tag{D-4}$$

respectively. Note that the auto-correlation does not include τ=0 shift since, when the codes are perfectly aligned (τ=0), the correlation becomes N. A tractable criterion for CDMA code selection is to minimize P_A and P_C for all possible time shifts, τ. It is noted that the selection of CDMA codes based on only the minimum P_A and P_C may not necessarily correspond to optimized system performance [12]. However, optimized system performance should always have small P_A and P_C and, hence, they are reasonable criteria for CDMA code design.

A lower bound for the maximum cross-correlation of any pair of binary sequences has been derived by Welch [24] and is given as

$$P_C \geq N\sqrt{\frac{M-1}{NM-1}} \tag{D-5}$$

where N is the period of the code and M is the available sequences' size. The Welch bound allows comparison of code cross-correlation properties with the theoretically achievable values. Note that for large period N, the lower bound is on the order of $\sqrt{N}$.

I. Family of CDMA Codes

The three families of binary ($\pm$1) CDMA codes that are favorable for deep-space communication are M-sequences, Gold sequences, and Kasami sequences.[1] The key characteristics of each of the sequences, such as the code period (N), the available code size (M) for a given shift register length (L), and the maximum auto- and cross-correlation values (P_A and P_C), are described below. Here we restrict ourselves to BPSK signals consisting of two phases ($\pm$1). In addition, we do not consider Bent sequences [12] for deep-space communications since the sequence generator for this code is more complicated than a simple feedback shift register. Moreover, the attractive anti-intercept property of Bent sequences is not needed for this application.

Each of the CDMA codes described here can be generated easily by one or more feedback shift registers. The shift registers produce output sequences (M-sequences, Gold sequences, or Kasami sequences) depending upon the register length, feedback tap connections, and initial shift register conditions. For example, Fig. D-1(a) shows a shift register of length L that can produce M-sequences. A detailed mathematical description of shift register sequences can be found in [25,26] and will not be described here.

Table D-1 summarizes the key characteristics of the M-sequences, Gold sequences, and Kasami sequences. The first family of CDMA codes described here consists of M-sequences. A characteristic of M-sequences is that they have a period of $N = 2^K - 1$, where K can be any positive integer number. The advantage of M-sequences is that the auto-correlation is always -1 (therefore, P_A=1), except for the case when the code positions are perfectly aligned, where it takes on the value N. The disadvantages are that

[1] Here we only consider the small set of Kasami sequences. The large set of Kasami sequences, in fact, contains both the small set of Kasami sequences and a set of Gold (or Gold-like) sequences as subsets [20]. Moreover, the maximum P_C and P_A values for the large set of Kasami sequences are identical to those of Gold sequences and, thus, are not discussed here [12].

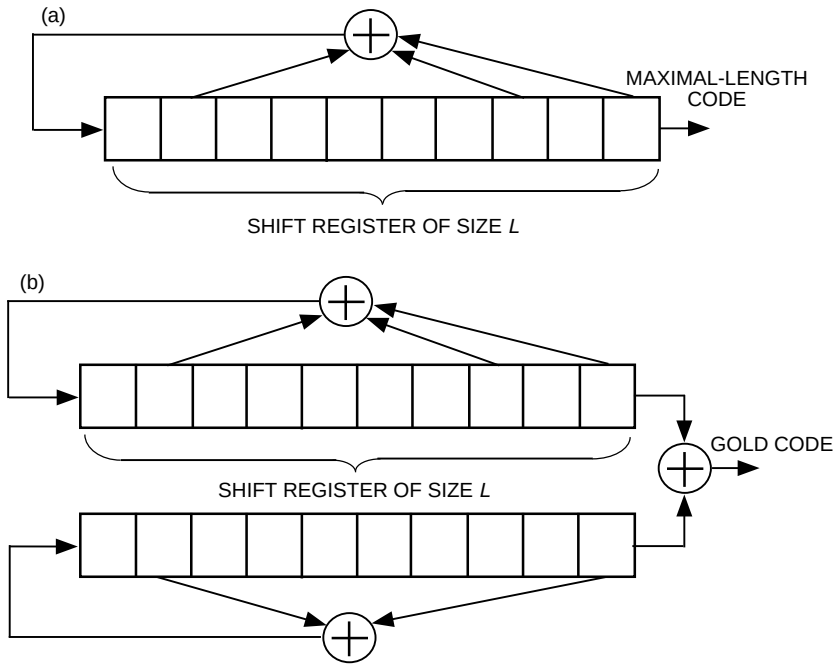

Fig. D-1. CDMA code generators producing (a) M-sequences and (b) Gold sequences.

Table D-1. Key characteristics of M-sequences, Gold sequences, and Kasami sequences.

Register length,	Code period,	M-sequences			Gold sequences			Kasami sequences		
L	N	M	P_C	P_A	M	P_C	P_A	M	P_C	P_A
3	7	2	5	1	9	5	5	—	—	—
4	15	2	9	1	17	9	9	4	5	5
5	31	6	11	1	33	9	9	—	—	—
6	63	6	23	1	65	17	17	8	9	9
7	127	18	41	1	129	17	17	—	—	—
8	255	16	95	1	257	33	33	16	17	17
9	511	48	113	1	513	33	33	—	—	—
10	1023	60	383	1	1025	65	65	32	33	33
11	2047	176	287	1	2049	65	65	—	—	—
12	4095	144	1407	1	4097	129	129	64	65	65

the cross-correlation values are poor as compared with the auto-correlation properties, and that the size of code grows slowly as the register length increases. More details of M-sequences and properties of shift register sequences can be found in [20].

The second family of described CDMA codes consists of Gold sequences. Gold sequences have been used for multiple access in the past by the Global Positioning System (GPS) and the Tracking and Data Relay Satellite System (TDRSS). Gold sequences [27] can be generated easily by properly combining the outputs of two feedback shift registers of length L, as shown in Fig. D-1(b). Similar to M-sequences, Gold

sequences also have a code period of $N = 2^K - 1$, where K can be any positive integer number. Gold sequences have their best cross-correlation when L is odd. The key advantage of Gold sequences over the other families is that the size of available Gold sequences is large, $(N + 2)$ for a given code period, N. Unlike M-sequences, Gold sequences have the same maximum auto- and cross-correlation properties. A good reference for Gold sequence construction is [10].

Finally, the third family of CDMA codes described here consists of Kasami sequences. Kasami sequences also have a length of $N = 2^K - 1$, but K can only be an even integer [12,28]. Similar to Gold sequences, the Kasami sequences can also be generated by a pair of feedback shift registers. As shown in Table D-1, Kasami sequences satisfy the Welch bound, which means that the Kasami sequences are optimal. The key disadvantage of Kasami sequences is that there are a limited number of them for a given even shift-register size (only $2^{L/2}$). Similarly to Gold sequences, the maximum auto- and cross-correlations of Kasami sequences are identical.

II. Comparison of Various Code Families

For a limited number of users, M-sequences are attractive due to their minimum auto-correlation properties. For communication systems with a limited number of users, M-sequences should be selected. Gold sequences, on the other hand, have good cross-correlation properties for odd L, but the worst ones for even L. The number of available codes for Gold sequences is the highest of the three families. Gold sequences should be selected when a large number of codes are required. Kasami codes have very small code sizes, but they achieve the Welch bound in cross-correlation. Kasami sequences should be used when a few number of codes is sufficient and when an even number of L is possible.

Appendix E

Code Division Multiplexing—Comparison of Options A and C

In this appendix, the difference between option A and option C of the proposed CDM uplink option in terms of the required power amplifier back off will be discussed. Since it is the peak-to-average power variation, instead of the absolute power, that determines the amount of back off, the unnormalized signal constellation can be used for illustration. The sampled multilevel composite signal at the nth WH code bit interval is (without the pilot signal)

$$z_n = \sum_{i=1}^{M} d_i(nT_b)W_i(nT_b)$$

which takes on one of the $M+1$ values from the set $\{-M, -M+2, \ldots, M-2, M\}$. The possibility that $z_n = |M - 2k|$ can be written as

$$P\{z_n = |M-2k|\} = \begin{cases} \binom{M}{M-k}\left(\frac{1}{2}\right)^M, & M = 2k \\ 2\binom{M}{M-k}\left(\frac{1}{2}\right)^M, & M \neq 2k \end{cases} \quad \text{(E-1)}$$

By assuming the pilot signal amplitude $A_0 = a$ in option A, the average power (unnormalized) can be derived from the one-dimensional signal constellation as

$$P_{Avg} = \sum_{k=0}^{\lfloor \frac{M}{2} \rfloor} \left(\frac{(a+M-2k)^2}{2} + \frac{(-a+M-2k)^2}{2} \right) P\{z_n = |M-2k|\}$$

$$= a^2 + \sum_{k=0}^{\lfloor \frac{M}{2} \rfloor} (M-2k)^2 P\{z_n = |M-2k|\}$$

$$= P_{\text{Pilot}} + P_{\text{Data}} \tag{E-2}$$

This result suggests that the average transmitted power is just a sum of the pilot signal power and the average data power, even though the pilot signal is directly added to the multilevel composite signal. Therefore, it can be easy to determine what $A_0 = a$ would be for a given percentage α of power allocated to the pilot signal by letting

$$\frac{P_{\text{Pilot}}}{P_{\text{Pilot}} + P_{\text{Data}}} = \alpha \tag{E-3}$$

The peak power (unnormalized) is

$$P_{\text{Peak}} = (a+M)^2 \tag{E-4}$$

so that the peak-to-average power variation is $P_{\text{Peak}}|_{dB} - P_{\text{Avg}}|_{\text{dB}}$.

For option C when the PN sequence on the quadrature channel has a relative amplitude a, the average power (unnormalized) can be derived from the two-dimensional signal constellation as

$$P_{Avg} = \sum_{k=0}^{\lfloor \frac{M}{2} \rfloor} \left(a^2 + (M-2k)^2 \right) P\{z_n = |M-2k|\}$$

$$= a^2 + \sum_{k=0}^{\lfloor \frac{M}{2} \rfloor} (M-2k)^2 P\{z_n = |M-2k|\}$$

$$= P_{\text{Pilot}} + P_{\text{Data}} \tag{E-5}$$

which is identical to the average power in option A. Similarly to option A, the amplitude a can be determined for any given α by Eq. (E-3). However, the peak power (unnormalized) becomes

$$P_{\text{Peak}} = a^2 + M^2 \tag{E-6}$$

which is smaller than the peak power in option A. Hence, the peak-to-average power variation for option C is smaller than that for option A, which in turn gives smaller power amplifier back off for option C.

Appendix F

Code Division Multiplexing—Walsh Functions With Majority Logic Multiplexing

In this section, the advantages and limitation of using Walsh functions for majority logic multiplexing will be summarized. The advantages of a majority logic multiplexing scheme are that (1) the transmitted signal is binary and (2) error correction capability is added as transmitted data are redundantly encoded. However, the nonlinearity introduced in such a scheme greatly limits the availability of suitable code sets for unambiguous mapping from the transmitted codeword to the demultiplexed codeword through a binary symmetric channel, in which hard decision is made on each bit of the received binary multiplexed signal before correlating with the local Walsh function reference. Extensive computer searching is used to find suitable code sets for binary symmetric channels, and only a limited number of them are found for a seven-user majority logic multiplexing scheme. According to [21], they include all shifts of a length-7 M-sequence and the set of truncated Walsh functions of length 7, which is formed from the regular length-8 Walsh function set with the leading bit truncated.

Further study on the truncated length-7 Walsh functions through our simulation indicates that this code set is actually not good for all the situations. For the cases when all seven or any N of the seven input streams to the multiplexer are active, where N=1, 2, 3, and 6, the truncated length-7 Walsh functions work well to ensure unambiguous mapping from each input stream to its corresponding demultiplexed stream at the receiving end. However, when only four or five input streams are active, one of them will get corrupted in most cases even though no error is made during transmission. Tables F-1 and F-2 summarize the occurrence of such a failure (in the format of corrupted channel:{list of inactive channels}) for five active input streams and four active input streams, respectively.

Table F-1. Occurrence of a corrupted stream: five active input streams.

W1:{2, 3}	W2:{1, 3}	W3:{1, 2}	W4:{1, 5}	W5:{1, 4}	W6:{1, 7}	W7:{1, 6}
W1:{4, 5}	W2:{4, 6}	W3:{4, 7}	W4:{2, 6}	W5:{2, 7}	W6:{2, 4}	W7:{2, 5}
W1:{6, 7}	W2:{5, 7}	W3:{5, 6}	W4:{3, 7}	W5:{3, 6}	W6:{3, 5}	W7:{3, 4}

Table F-2. Occurrence of a corrupted stream: four active input streams.

W1:{2, 4, 7}	W2:{1, 4, 7}	W3:{1, 4, 6}	W4:{1, 2, 7}	W5:{1, 2, 6}	W6:{1, 2, 5}	W7:{1, 2, 4}
W1:{2, 5, 6}	W2:{1, 5, 6}	W3:{1, 5, 7}	W4:{1, 3, 6}	W5:{1, 3, 7}	W6:{1, 3, 4}	W7:{1, 3, 5}
W1:{3, 4, 6}	W2:{3, 4, 5}	W3:{2, 4, 5}	W4:{2, 3, 5}	W5:{2, 3, 4}	W6:{2, 3, 7}	W7:{2, 3, 6}
W1:{3, 5, 7}	W2:{3, 6, 7}	W3:{2, 6, 7}	W4:{5, 6, 7}	W5:{4, 6, 7}	W6:{4, 5, 7}	W7:{4, 5, 6}

Note that the truncated length-7 Walsh functions always fail when only five input streams are active, but may fail with 80-percent probability when four input streams are active. This is an interesting finding that was never mentioned in [30]. It is also confirmed through simulation that the regular length-8 Walsh functions can be used for the seven-user majority logic multiplexing scheme as long as the system is fully loaded or, in other words, all the input streams to the multiplexer are active at the same time. This ambiguity problem can be alleviated by using redundant data streams to keep all or relevant channels active, at the expense of not being able to take advantage of the error correction capability, as discussed later.

The built-in error-correcting capability of majority logic multiplexing using truncated Walsh functions is discussed in [30] by comparing the error rates of the multiplexed symbol and the correlator output channel symbol, with an assumption of a binary symmetric channel. In other words, a hard decision is made on each of the received multiplexed symbols before it is passed to the correlator. The system diagram of the simulation using the binary symmetric channel model is depicted in Fig. F-1(a), where the multiplexed binary signal formed from each of the 2^n symbol patterns (n active users) is corrupted by all the 2^7 equally likely error patterns (length-7 truncated Walsh functions), and the errors encountered in each receiving channel are counted and averaged over all equally likely symbol patterns. With the cases of four or five active input streams, which render ambiguous mapping excluded, the symbol error performance of majority logic multiplexing using truncated Walsh functions is summarized in Table F-3, where, with R_c being the multiplexed symbol SNR,

$$P_b = \frac{1}{2}\text{erfc}\left(\sqrt{R_c}\right)$$

is the error probability of making hard decision on each bit of the multiplexed binary signal on the receiving end. It is clear that, from Table F-3, the channel symbol error performance is improved significantly when the system is underloaded. However, the error performance in terms of channel symbol SNR, $R_s = 7R_c$ in this length-7 truncated Walsh functions case, shows a less rosy picture. Figure 14 shows a comparison with ideal BPSK error performance.

The system diagram of the simulation using an additive Gaussian noise channel is depicted in Fig. F-1(b), where a multiplexed binary signal is corrupted by white Gaussian noise and no hard decision is made on each bit of the multiplexed binary signal. We refer to this as the soft decision system, in comparison with the hard decision one using the binary symmetric channel model. The symbol error performances for both hard decision and soft decision systems are plotted in Fig. F-2 for comparison. The soft decision system outperforms the hard decision one when the multiplexer is underloaded. For a highly loaded system, the soft decision system performance fails to meet that of the hard decision system. The reason for this reversal is not clear and is still under study.

Table F-3. Symbol error performance of majority logic multiplexing using truncated Walsh functions.

No. of active input streams	Symbol error probability
1	$35P_b^4$
2	$7.7P_b^2$
3	$7.7P_b^2$
6	$2.2P_b$
7	$2.2P_b$

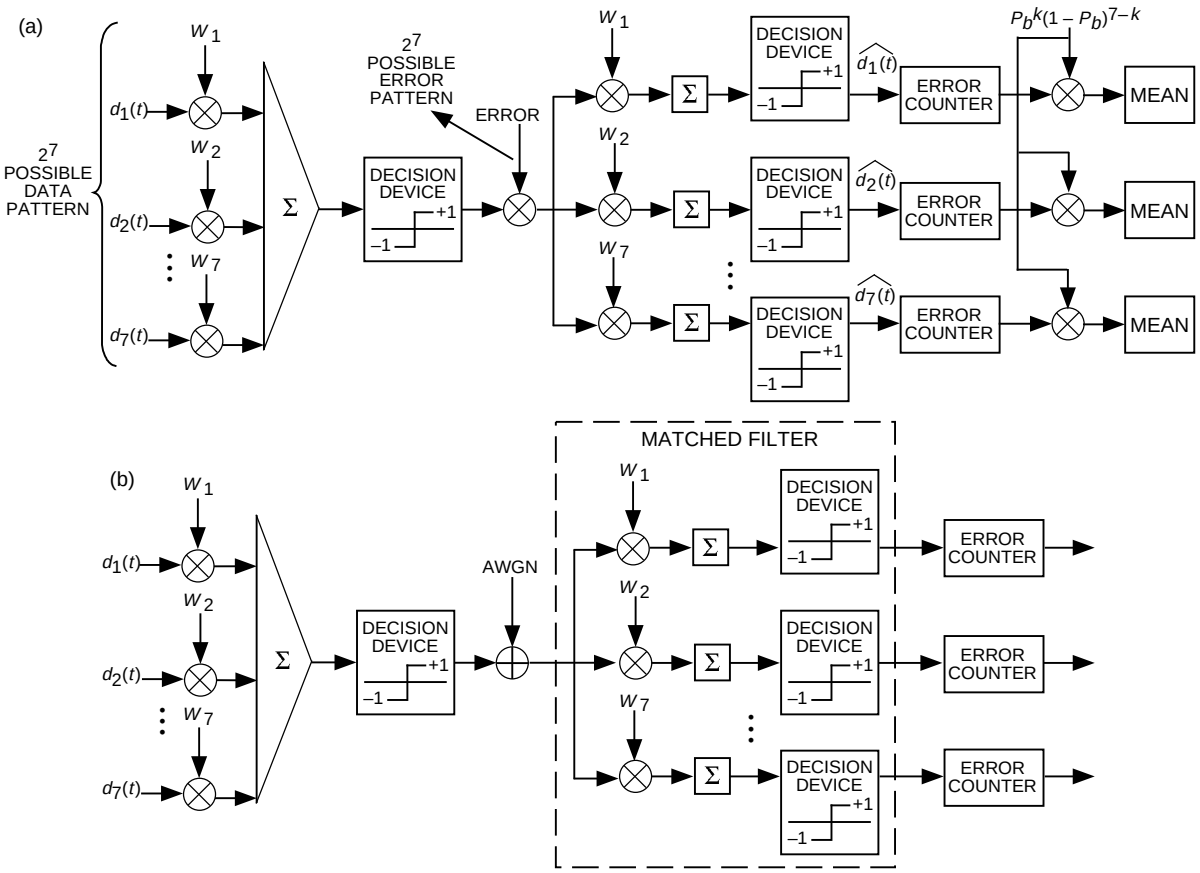

Fig. F-1. Simulation setup: (a) hard decision and (b) soft decision.

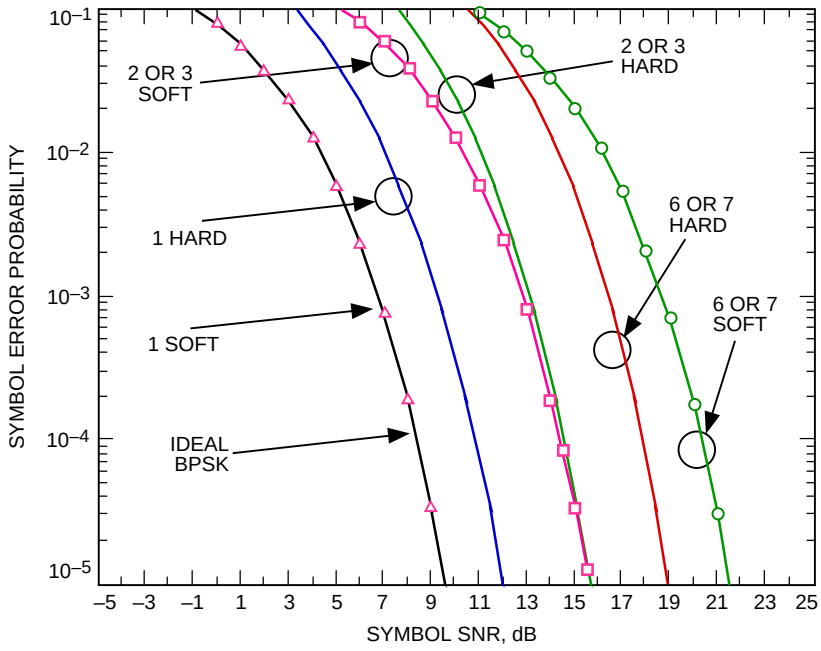

Fig. F-2. Comparison of SER performance for Walsh–Hadamard majority logic multiplexing schemes.